

Accounts

A Biomimetic Approach for Hierarchically Structured Inorganic Crystals through Self-Organization

Hiroaki Imai,* Yuya Oaki, and Akiko Kotachi

Department of Applied Chemistry, Faculty of Science and Technology, Keio University, 3-14-1 Hiyoshi, Kohoku-ku, Yokohama 223-8522

Received April 10, 2006; E-mail: hiroaki@applc.keio.ac.jp

Here, we describe a biomimetic pathway for the synthesis of hierarchically structured inorganic crystals. In artificial systems mimicking biomineralization, versatile morphogenesis was achieved with the construction of bridged nanocrystals through self-organization by controlling growth with polymeric molecules such as a gel matrix and soluble anionic polymers. The self-organized formation of bridged crystals in hierarchical architectures is a possible new paradigm for advanced materials processing which could afford new inorganic–organic nanocomposites for use as novel functional materials.

1. Introduction

Traditionally, crystal growth has involved the fabrication of homogeneous, large-sized single crystals.[1] A wide variety of crystal growth techniques via solid, liquid, and vapor phases have been developed for the production of high quality crystals of functional materials utilized in electrical, optical, and mechanical applications. Large-sized single crystals are commonly processed into small devices using microfabrication techniques. Especially, the miniaturization for electronics became possible due to the recent development of "top-down" approaches, such as photolithography. However, the conventional top-down fabrication methods are becoming extremely complicated and approaching the physical limits of the miniaturization processes for nanoscale electronic circuits and mechanical devices.

Hierarchic biomaterials are spontaneously produced through "bottom-up" processing by life, and in recent years, it has inspired bottom-up chemical approaches to various novel nanomaterials and nanostructures. In particular, biominerals, which are directly produced in an aqueous solution system at ambient atmosphere, are an excellent example of advanced inorganic and inorganic–organic composite materials. Very recently, a hierarchy of biominerals has been reported to be constructed with nanoscale building blocks.[2,3] Therefore, biomineralization and biomimetic routes have attracted much attention in the research fields of materials chemistry and nanotechnology as a smart technique for the fabrication of nanoscale functional materials.

In biomineralization process, the production of inorganic crystals, including macroscopic morphology, microstructures, polymorphs, orientation, crystallinity, and nucleation sites, is known to be strictly controlled by biological organic molecules.[4] Thus, biomimetic approaches for crystal growth has been studied using various kinds of organic molecules and molecular assembly.[5–15] Morphogenesis with coexisting molecules has been reported by many research groups as well as the control of the nucleation sites with specific organic surfaces, including polymer films and self-assembled monolayers. Emergence of complex and hierarchical architectures of inorganic crystals through self-organization has been found in aqueous solution systems.[16–21] However, morphological evolution has not been systematically investigated although the self-organized formation of inorganic crystals is essential for understanding biomineralization and developing biomimetic materials processing.

In this article, morphogenesis in biomineralization is discussed on the basis of crystal growth by self-organization as well as the clarification of the elaborate nanoscale structures of biominerals. Then, we describe biomimetic pathways for complex shapes of inorganic crystals through the macroscopic and microscopic self-organization using gel matrices and/or capping agents. Self-organized crystal growth was found to be controllable with organic templates under diffusion-controlled mass transport. The elucidation and the combination of these strategies are likely to be a pivotal aspect in designing hierarchical architectures of inorganic crystals with cooperative organic agents.

2. Self-Assembly or Self-Organization? Morphogenesis on Crystal Growth

These days, "self-assembly" and "self-organization" are popularly used for spontaneous ordering, including the formation of spatial patterns and temporal oscillations.[22] However,

Published on the web December 13, 2006; doi:10.1246/bcsj.79.1834

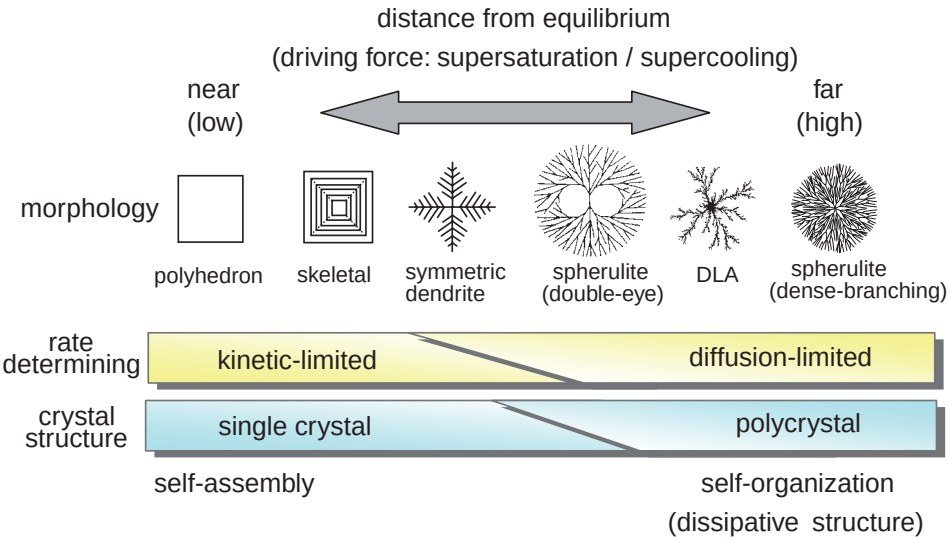

Fig. 1. Self-assembly and self-organization on morphological variation of crystals.

the definition of these words is obscure to the general public. In self-assembly, static and stable order forms near equilibrium and has periodicity and symmetry derived from the components of a system. The formation of supramolecules through hydrogen bonds and molecular aggregates, such as micelles and Langmuir–Bloddget films, is categorized as self-assembly. On the other hand, self-organization, which is also called "dissipative structure," is ordering at far-from-equilibrium, and the resultant pattern is not associated with the size and symmetry of the components. A convection pattern in a Rayleigh–Benard system and an oscillation in a Belousov–Zhabotinski reaction are typical dissipative structures. Spatiotemporal patterns in dissipative structures are usually maintained by heat and mass flow in a non-equilibrium open system.

Crystallization is the spontaneous formation of a microscopic, periodic array of atoms, ions, or molecules and may be categorized as self-assembly or self-organization. The patterns formed during crystallization are basically affected by the distance between the growth conditions and the equilibrium state,[1,23] i.e., the driving force for the crystallization, such as the degree of supersaturation and the supercooling (Fig. 1). Polyhedral forms are obtained when crystal growth occurs near the equilibrium state. Since the macroscopic shape of the polyhedrons reflects the arrangement and the symmetry of the microscopic atomic or molecular lattice, which is a component of the system, crystallization is categorized as self-assembly. As the driving force increases, the growth rate is governed by mass diffusion or heat transfer, and then, the growing surface becomes unstable in a diffusion field. Under these conditions, dendrite forms with a complicated period structure are produced by the competition between the promotion and suppression of the crystal growth. When the driving force greatly increases, random polycrystals, exhibiting spherulite and diffusion-limited aggregate (DLA), are formed with a disappearance of the crystallographic symmetry. The crystallization process of various morphologies, which depend on the environment, including the driving force of the crystallization and the diffusion rate of the components, should be categorized as self-organization. However, the dissipation of energy with heat and mass flow is not required for the maintenance of the organized patterns because the crystal structure as a product of self-organization is solidified.

Morphogenesis and pattern formation of life have been studied as self-organization at far-from-equilibrium. On the other hand, the formation of supramolecular structures of biological molecules, such as the double helix of DNA and folding of proteins, is categorized as self-assembly near equilibrium. Consequently, the hierarchy in a living body is considered to be constructed by microscopic self-assembly and macroscopic self-organization. Furthermore, pattern formation in biomineralization can be discussed on the basis of self-assembly and self-organization. This viewpoint is important for understanding the mineralization process in a living body and reproduction of the biomimetic architectures in artificial systems. In general, biomineralization involves four steps:[4a] (I) initiation of crystallization by supersaturation in a specific space with mass transport, (II) direction of the nucleation with a specific organic substrate, (III) modulation of crystal growth with adsorption of specific organic molecules, and (IV) integration of the resultant crystals into intra- and inter-cellular network structures (Fig. 2). Because cellular cytoplasm consists of a gel or a viscous solution, mass transport during the mineralization process should be controllable by the organic matrix. The direction of the nucleation sites for the crystallization is ascribed to molecular recognition between an inorganic crystal and an organic substrate as a template. Self-organized formation of inorganic crystals is known to be modulated by adsorption of specific organic molecules. The concept of recognition between an organic molecule and an inorganic crystal surface has been explored for habit modification with the specific adsorption on a specified crystal face. Consequently, steps I, II, and III may be achieved by controlling self-assembly and self-organization during crystal growth. Emergence of self-organization with a matrix and organic molecules and the control of the organization with a template are important to the formation of biomimetic hierarchical architectures in inorganic crystals similar to real biominerals. On the other hand, the reproduction of step IV in an artificial system seems to be

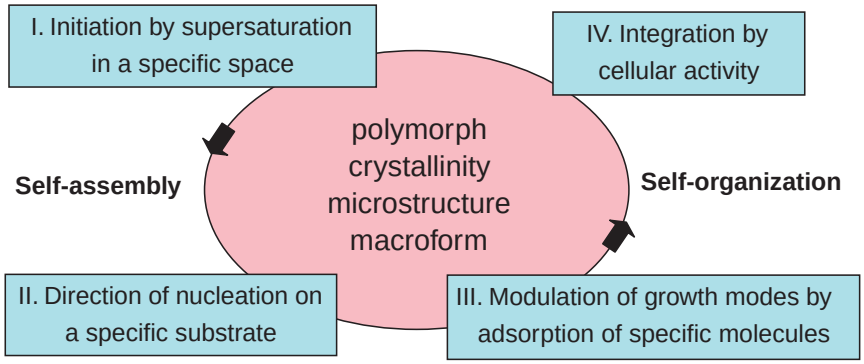

Fig. 2. Four steps for control of crystal growth in biomineralization.

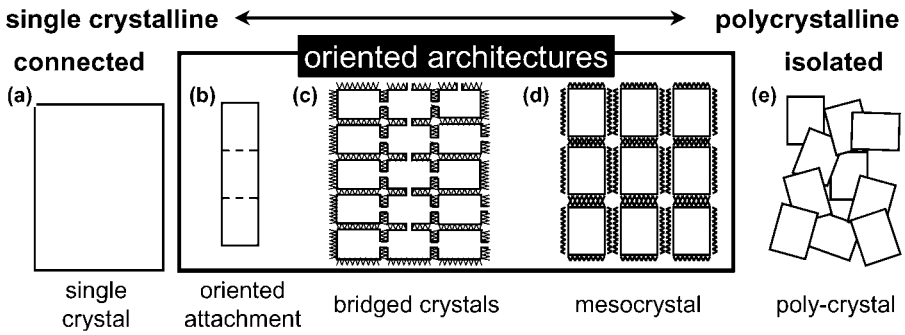

Fig. 3. Classification of intermediate states between single crystal and polycrystal. Oriented attachment and bridged crystal may be categorized into single crystal. Bridged crystal and mesocrystal are fundamentally covered with molecular species which could accept organic molecules.

difficult because intra- and inter-cellular network structures are governed by complex biological activities.

3. Single Crystal or Polycrystal? Understanding Hierarchical Architecture of Biominerals

Very recently, some evidence has been reported that many crystallization events are not categorized as classical single crystals and polycrystals (Fig. 3).[24–26] Some intermediates, called mesocrystals, are an assembly of nanocrystals into superstructures with an ion or molecule attached to a critical crystal nucleus. Subsequent crystallographic fusion of mesocrystals can lead to single crystals with a preserved shape. Direct nanoparticle fusion, based on a mechanism of an oriented attachment, can directly lead to single crystals. By considering biominerals with their often complex forms and several levels of hierarchy, a view of particle-mediated crystallization events can be developed.

The structure of biominerals has attracted the interest of researchers in a broad range of chemistry disciplines.[27–55] Although the architecture is a large, single crystal of calcium carbonate with occlusion of biopolymers, much remains unknown about the single crystal, especially in terms of the curved morphology surrounded by smooth surfaces, the coloration of the architecture, and the high mechanical strength, which prevents cleavage. Recently, biominerals including bones,[4a,4e] nacreous layers of seashells,[56] stereom of sea urchin spines,[57] diatoms,[58] and iron-oxidizing bacteria,[59] have been reported to be constructed of nanoscale building blocks. We have proposed that bridged nanocrystals with incorporation of organic polymers occur in real biominerals.[60–63] Specific macroscopic morphologies in biominerals of seashells, corals, echinoderms, and eggshells were found to consist of the oriented architecture of the nanocrystals that are 20–100 nm in size. Typical SEM (scanning electron microscope) and TEM (transmission electron microscope) images of a nacreous layer of Japanese pearl oyster (*Pinctada fucata*) and a spine of the sea urchin (*Echinometra mathaei* (*Blainville*)) on macroscopic and microscopic scales are shown in Fig. 4. Each biomineral represented the characteristic morphologies in macroscopic scales. The magnified SEM images of the fractured surface reveal the presence of nanoscopic structures. The assembly of nanocrystals was recognizable on the TEM images, indicating that the inside consisted of nanocrystal blocks. Each nanoblock was considered a single crystal because lattice images of the respective units corresponding to aragonite (the nacreous layer) and calcite (the sea urchin spine) were observed (not shown). The sizes of aragonite- and calcite-type nanocrystals were approximately 20–180 and 10–80 nm, respectively. Interestingly, the nanocrystals had various morphologies and crystal structures beyond the species barrier. These facts indicate that the integration of nanocrystals could be an important process for crystal growth in biomineralization.

Oriented architectures are bridged nanocrystals with incorporation of biopolymers because bridging is essential for the crystallographic connection. A macroscopic mineral bridge reportedly forms in the interlayer of mother-of-pearl.[32] Since the daughter aragonite plate is directed on the mother one through the formation of a mineral bridge, the orientation of the *c* axis

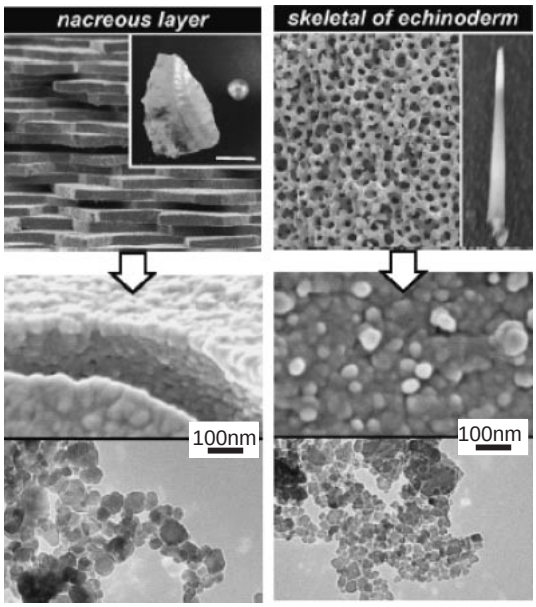

Fig. 4. Typical SEM and TEM images of biominerals in macroscopic and microscopic scales.[60,61]

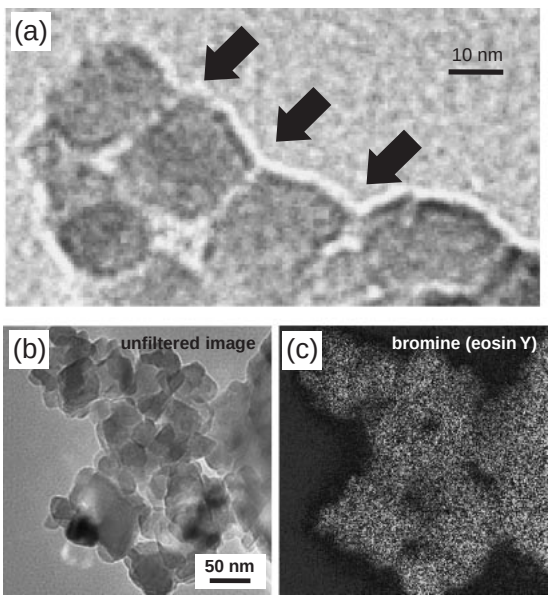

Fig. 5. Typical TEM images indicating nanoscopic mineral bridges (a) and homogeneous dispersion of dye molecules (eosin Y) (b, c) on nanocrystals in a sea urchin spine. White dots show the presence of bromine in eosin Y.[61] Reproduced from Ref. 61 with permission of Wiley-VCH.

perpendicular to the plates is inherited in a late stage of growth. Here, nanoscale mineral bridges between two adjacent nanocrystals were observed in TEM images (Fig. 5a). According to these facts, the oriented architecture of nanocrystals in biominerals can be ascribed to a bridged-growth process similar to mother-of-pearl.

Anionic dyes (eosin Y, Rhodamine B) and a hydrophobic dye (pyrene) were successfully introduced into calcite and aragonite blocks by immersion in an ethanol solution of the organic dyes for one day. Strong emission from the included dye molecules was observed with ultraviolet-light excitation, suggesting that the organic dyes were incorporated in a specific state surrounded by organic molecules. Homogeneous dispersion of the dye molecules was confirmed by the detection of bromine in eosin Y molecules using energy-filtered mapping and an electron energy loss spectrum (Figs. 5b and 5c). These results indicate the presence of biopolymers, which were incorporated with the dye molecules, at the interface of the nanocrystals. Thus, the bridged nanocrystals covered with biopolymers in biominerals are a nanoscopically intertwined inorganic–organic composite.

These findings imply that the complex morphologies of biominerals can be designed by bridged nanocrystals (Fig. 3) via the self-organization in association with biopolymers. A batch of bridged nanocrystals is fundamentally a single crystal incorporating organic molecules. However, nonconformity or twin formation gradually increases at the nanobridges. Using nanocrystals as building blocks, versatile morphological design on macroscopic scales can be performed, especially in terms of complex or curved shapes with smooth surfaces. Simultaneously, the bridged structure led to an oriented architecture that cannot simply be classified as a single- or polycrystalline material. In addition, a nanocomposite of inorganic crystals and organic polymers provides molecular storage of organic guest molecules. If the stereom is a perfect single crystal, the dye molecules would not be included in the architecture. These results strongly indicate that the molecular storage of organic molecules, which is associated with the coloration of biominerals, is possible with a nanocomposite constructed from bridged inorganic bricks and biopolymer mortars. Finally, we elucidated the hierarchical architecture in biominerals and identified their ability to host organic molecules, which we have termed "nanostorage."

4. Emergence of Self-Organization in a Gel Matrix

4.1 Morphological Variation Depending on Gel Density. The oriented architectures occur because of the connection between crystals, and formation of the hierarchical crystals is attributed to the sequential growth through mineral bridges. Here, we describe morphological control of self-organization of macroscopic bridged structures in a gel. A gel matrix has been used for the control of nucleation and morphology on aqueous solution-based crystal growth.[64–68] In the initial stage, various inorganic crystals were produced in various gels because the media provide appropriate conditions for the growth of large defect-free single crystals.[64] The advantage of gel media is believed to be the reduction of the nucleation rate and suppression of convection. Recently, we experimentally demonstrated the systematic variation of crystal morphology by varying the density of the gel matrix (Fig. 6).[69] The morphological evolution of the inorganic crystals ($Ba(NO_3)_2$, NH_4Cl, H_3BO_3, and $K_2Cr_2O_7$) was demonstrated in various kinds of organic gel media (agar, gelatin, pectin, and poly(vinyl alcohol)). As the gel density increased, the morphology grown in the gel matrix changed remarkably from polyhedral single crystals exhibiting specific habits into dendritic forms consisting of irregularly branched polycrystalline aggregates, regardless of the sorts of inorganic compounds and gelling agents. The change from polyhedrons into dendrites via skeletal forms

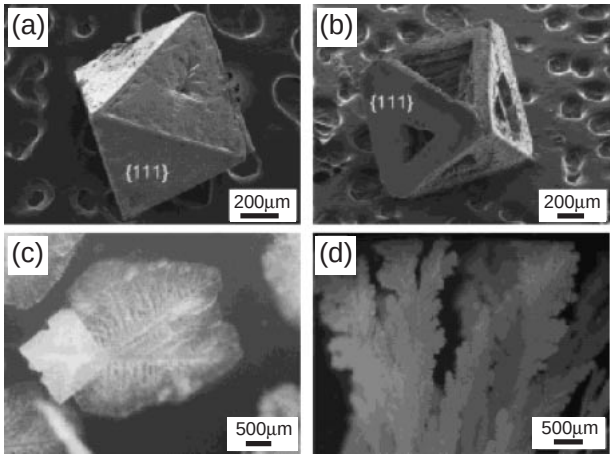

Fig. 6. Experimental changes in crystal morphology by varying the density of gel matrix.[69] Optical microscope (OM) and SEM images show morphological evolution of $Ba(NO_3)_2$: (a) regular octahedron at $C_{Ba} = 15/C_{ag} = 0.4$, (b) skeletal form at $C_{Ba} = 15/C_{ag} = 1.0$, (c) regular dendrite at $C_{Ba} = 15/C_{ag} = 2.0$, and (d) $C_{Ba} = 15/C_{ag} = 8.0$. C_{Ba} and C_{ag} indicate the initial concentrations (g/100 g of water) of $Ba(NO_3)_2$ and agar, respectively. Reproduced from Ref. 69 with permission of the American Chemical Society.

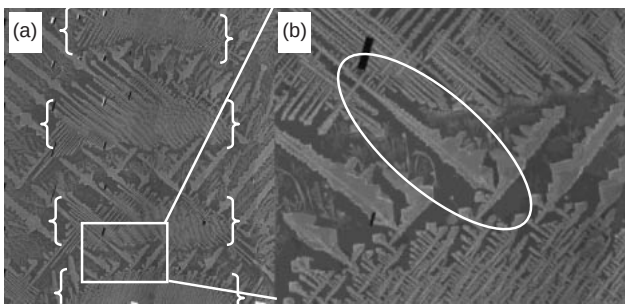

Fig. 7. OM images show for two-dimensional dendrites of NH_4Cl grown in agar gel. Oriented dendrites were periodically produced in the gel matrix (a). The dendrites were crystallographically connected through a bridge (b).

is ascribed to an increase in the influence of diffusion of the solutes on the crystal growth. Since gel media generally suppress the mobility of ions, densification of the media decreased the apparent diffusion rate of the solutes and finally promoted the formation of diffusion-controlled morphologies including skeletal, dendritic, and branched forms (matrix effect).

As shown in Fig. 7, we found a periodic production of dendrites of NH_4Cl in a thin layer of agar gel. Interestingly, the crystallographic orientation of these dendrites was almost the same although a slight deviation of the direction was occasionally observed. Due to the presence of a bridge between the dendrites having the same orientation, the crystal growth occurred sequentially through the macroscopic bridges. Consequently, the self-organized formation of periodic dendritic morphologies is associated with bridged crystals which can be macroscopically identified.

If the degree of supersaturation or the gel density is low, polyhedral shapes are formed through self-assembly (Fig. 1). The morphogenesis of the geometric shapes is restricted because they are thermodynamically stable. On the other hand, the orderliness and controllability of random aggregates are quite low if there is a high degree of supersaturation or if the gel matrix is very dense. Self-organization that is induced under an intermediate condition would produce various complex structures by integration of unit crystals because the combination of appropriate order and flexibility is achieved through crystallographic connections. The emergence of self-organization based on a balance between the crystal growth and the mass transport controlled with the gel matrix is an essential factor for the control of the morphogenesis.

4.2 Helical Morphologies Grown in Gel. Here, a model case for versatile morphogenesis in macroscopic scales using gel matrix is described. Helical and spiral architectures, which are fundamental shapes exhibiting chirality, were observed on various scales in nature. Their unique morphology is fascinating, and the formation mechanisms for many kinds of helical forms are still in a mystery. Biological polymers and designed macromolecules produce helical molecular assemblies from the nanometer to the submicron scale with a specific interaction through hydrogen bonding.[70] Macroscopic helical morphologies have also been observed with organic molecules,[71] polymers,[72] and inorganic materials[73–78] without microscopic chirality.

We found that the formation of peculiar curved and helical branches in dendrites occurs in triclinic crystals (H_3BO_3, $K_2Cr_2O_7$, and $CuSO_4 \cdot 5H_2O$) grown in a gel (Fig. 8).[79] The formation of the chiral architecture from achiral components occurs due to rotated accumulation of tilted units under conditions of diffusion-limited growth. Thus, the formation model proposed here would be applicable to various helical architectures and complex morphologies, including twisted ribbons in polymer spherulites. The results, described herein, provide novel guidelines for the morphogenesis of various helical and twisted forms. This is an excellent example for the variation from self-assembly into self-organization on the crystal growth in a gel matrix (Fig. 9). The helical structures would be formed by sequential growth of the tilted units through a bridge under diffusion-controlled mass transport in a gel. In this case, however, the crystallographic orientation deviated at a constant angle, like twinning.

The concept of stereochemical recognition between a chiral molecule and an inorganic crystal surface has been explored over the past decade.[80–84] Habit modification with stereochemical adsorption of a chiral molecule on a specified crystal plane has also been experimentally demonstrated.[82,83] We found a new type of morphological chiral tuning for inorganic helical crystals through stereochemical recognition of organic molecules.[85] The proportion of the right- and left-handed helices was precisely tuned with the addition of a specified amount of chiral molecules such as D- and L-glutamic acids (Figs. 8e and 8f). The chiral molecules were recognized by the enantiomeric surface of the triclinic crystal and then changed the growth behavior of the right- and left-handed helical morphology. Consequently, microscopic chiral information at a molecular level was amplified into the macroscopic helices consisting of inorganic achiral components. This phenomenon is the control of the self-organization on the crystal growth with spe-

cific adsorption of organic molecules (Fig. 9). In the following section, a capping effect by polymeric molecules on self-organization during crystal growth is described.

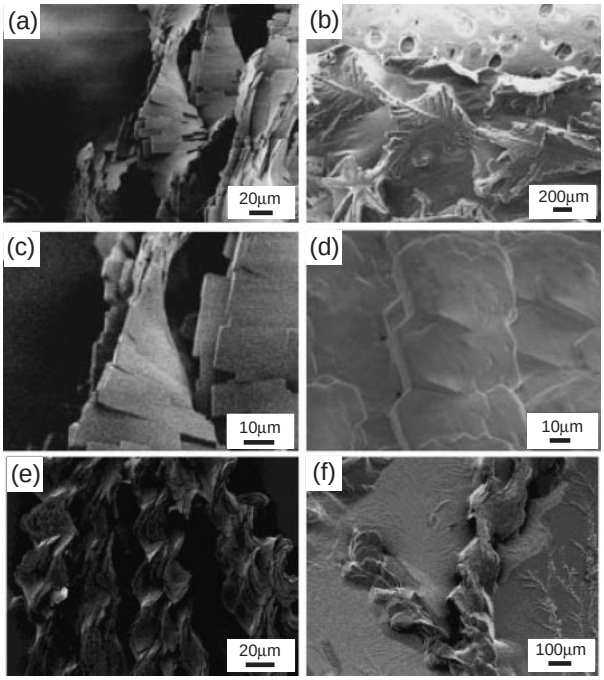

Fig. 8. Helical branches in dendrites with crystals ($K_2Cr_2O_7$ and H_3BO_3) grown in gel.[79,85] SEM images of (a, c) $K_2Cr_2O_7$ in pectin ($C_{KC} = 3.0$, $C_{pe} = 0.3$) and (b, d) H_3BO_3 in agar ($C_{HB} = 2.0$, $C_{ag} = 0.2$). C_{KC}, C_{BH}, C_{pe}, and C_{ag} indicate the initial concentrations (g/100 g of water) of $K_2Cr_2O_7$, H_3BO_3, pectin, and agar, respectively. Typical right-handed (e) and left-handed (f) helices in gel obtained by evaporation of water. Reproduced from Refs. 79 and 85 with permission of Wiley-VCH and the American Chemical Society.

5. Emergence of Self-Organization with Soluble Polymeric Agents

5.1 Growth of Calcium Carbonate in Cooperation with Poly(acrylic acid). 5.1.1 Formation of Bridged Nanocrystals and Development on Films with a Microscopic Template: As mentioned above, the control of crystal growth using soluble agents is an essential factor for biomineralization. Since calcium carbonate ($CaCO_3$) is one of the most well-known biominerals, the growth of the carbonate crystals has been widely demonstrated using various organic molecules and templates. The typical approach is habit modification leading to morphological evolution of precipitates using polyelectrolytes.[17] Rigid templates and patterned molds are used for the production of porous, carbonate mimicking biogenic structures.[86–88] Microemulsions and gelatin molecules also induce porous vaterite architectures.[89,90] Poly(acrylic acid) (PAA), which is a simple linear polymer having carboxy groups, is commonly utilized as a soluble agent to modify the crystal structure. The formation of $CaCO_3$ films on an insoluble organic substrate in the presence of PAA has been investigated by many researchers.[9–11,91–93] However, the influence of the polyelectrolyte on the morphology of $CaCO_3$ crystals has not been sufficiently clarified because morphological evolution required the coexistence of the organic substrates in most of the previous studies. We systematically investigated the influence of the concentration and the molecular weight of PAA on the morphological evolution of $CaCO_3$ grown on a simple glass substrate in order to clarify the performance of the polymeric molecules.[93]

As shown in Fig. 10a, calcite generally exhibits rhombohedral facets surrounded with {10–14} in the absence of any additives. Round crystals were obtained by the addition of low-molecular-weight PAA (PAA2k, Mw: 2000) (Fig. 10b). Small triangular calcite grains of less than 1 μm, which were arranged in the same orientation, were found on the round crystals (Fig. 10c). Based on thermogravimetry, the content

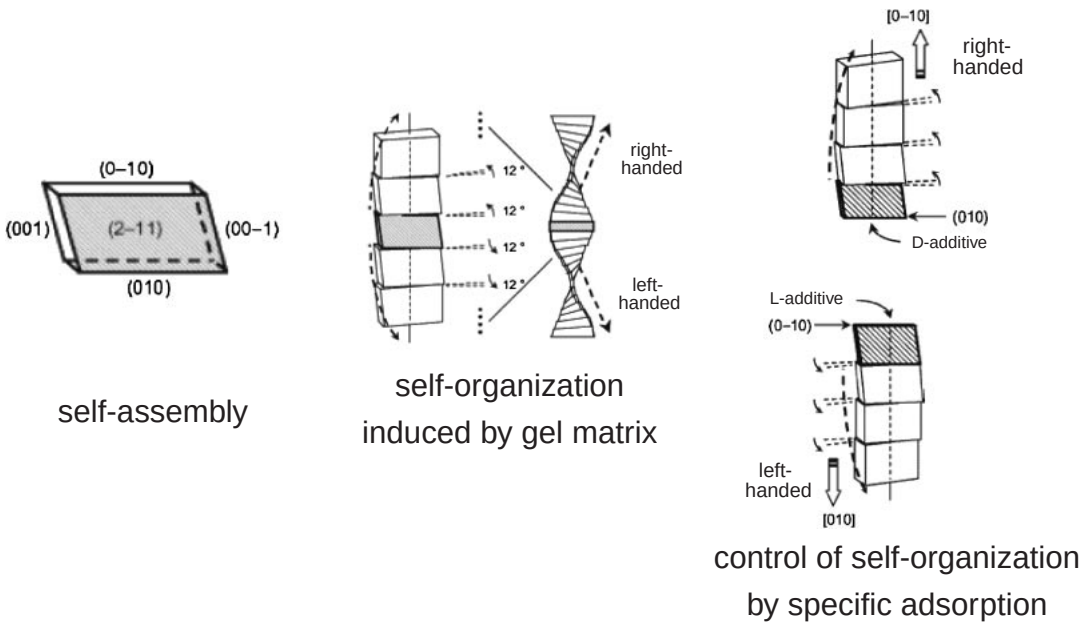

Fig. 9. Self-assembly and self-organization of crystals with a helical morphology.

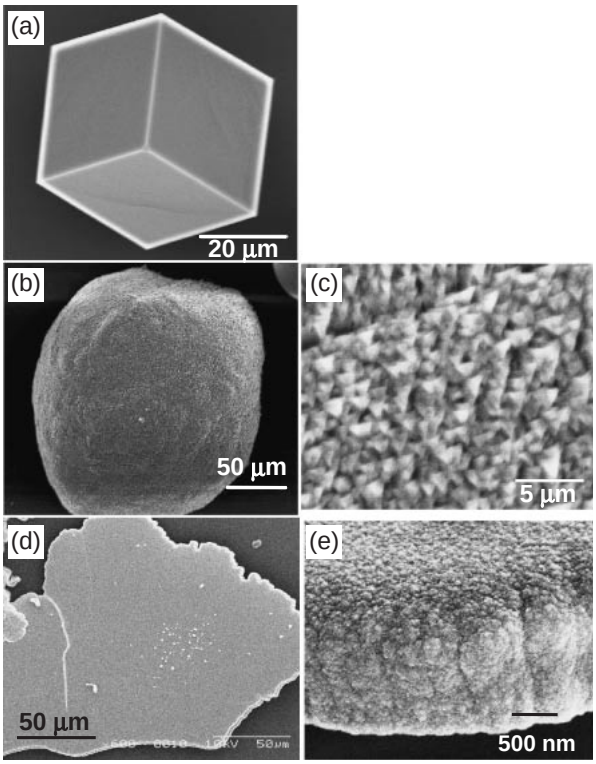

Fig. 10. Calcite crystals grown in the presence of PAA.[93] SEM images of calcite obtained in the absence (a) and in the presence of PAA: (b, c) $C_{Ca} = 20\,mM$, $C_{PAA2k} = 7.2 \times 10^{-2}$ wt % (10 mM) for 3 days and (d, e) $C_{PAA250k} = 7.2 \times 10^{-2}$ wt % (10 mM) for 3 days. Reproduced from Ref. 93 with permission of the American Chemical Society.

of PAA in/on the calcite crystals grown in the solutions increased with an increase in the PAA concentration. These facts suggest that the presence of PAA2k molecules suppressed the regular crystal growth through adsorption on specific surfaces of calcite and then induced the formation of small, bridged grains on the basal crystal (capping effect). The small triangular grains were inferred to be surrounded with the {10–14} faces covered with the polymers.

Planar films were formed on a glass substrate with a large amount of high-molecular-weight PAAs (PAA90k, Mw: 90000 and PAA250k, Mw: 250000) (Fig. 10d). Extremely small grains were found in the films by SEM observation (Fig. 10e), and crystallites of calcite with a size of 5–10 nm were seen by TEM. Planar films consisting of nanoscale grains were found to contain 3–4 wt % of the organic compound. These facts suggest that the specific adsorption of PAA chains highly suppressed the regular growth of calcite crystals, and then the morphology changed from polyhedral to a bridged architecture of miniaturized crystal units. An increase in the capping effect of PAA is ascribed to a higher adsorbability of molecules having a higher molecular weight. In the previous reports, the formation of PAA-mediated films required the presence of specific surfaces, such as a porphyrin monolayer,[14] chitin derivatives,[5,9] and PVA,[11] as templates. Thus, planar morphology could be achieved by the combination of the capping effect of the soluble agent and the template effect of the

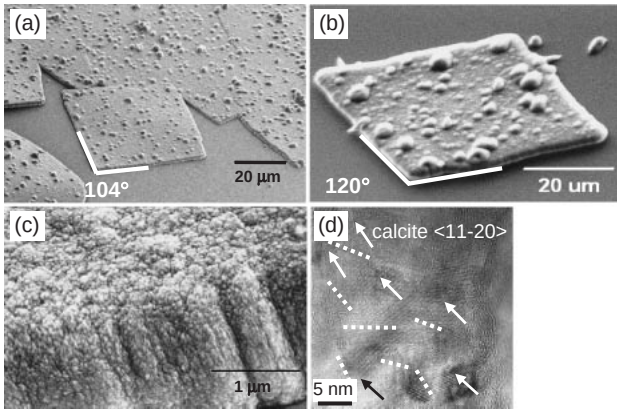

Fig. 11. Lozenge films of calcite grown in the presence of PAA.[93] Electron micrographs of calcite obtained in the presence of 7.2×10^{-2} wt % PAA250k and 2.4×10^{-3} wt % PAA2k (a–c). TEM image of the lozenge-shaped films (d). The lattice equidistances were assigned to the calcite {11–20} planes ($d = 2.495$ Å). Arrows and broken lines indicate the ⟨11–20⟩ direction and the grain boundary, respectively. Reproduced from Ref. 93 with permission of the American Chemical Society.

insoluble substrate promoting macroscopic two-dimensional growth. On the other hand, the presence of PAA90k and 250k induced the formation of $CaCO_3$ films even on a glass substrate without a coating of an insoluble species. Moreover, the specific combination of low- and high-molecular-weight PAAs (10 mM PAA250k and 0.33 mM PAA2k for 20 mM $CaCl_2$) produced lozenge-shaped calcite films with definite edges in a solution (Figs. 11a and 11b). Most of the parallelograms showed angles of 104 and 120°, corresponding to the shape of the {10–14} and {0001} faces, respectively. The XRD peaks due to the (10–14) and (0006) planes of calcite were distinct for these samples. Although the lozenge-shaped films exhibited regular crystallographic habits, small grains less than 100 nm were observed on the surface (Fig. 11c). These facts indicate that the crystal grains in the lozenge-shaped films were arranged two-dimensionally with a specific crystallographic orientation in which the ⟨10–14⟩ or [0001] direction was perpendicular to the substrate. As shown in a TEM photograph (Fig. 11d), there are lattice images of the {11–20} planes in the nanocrystals in the films. The ⟨11–20⟩ directions of the lattice (arrows) were slightly shifted at the grain boundaries (white broken lines).

Low-molecular-weight PAA (Mw: 2000) weakly suppressed the regular crystal growth and miniaturized calcite grains as a capping agent. The specific interaction is ascribed to the similarity of the distance of carboxy groups of a PAA molecule to that of calcium anions on the {10–14} plane of $CaCO_3$ (Figs. 12a and 12b). The oriented architectures are composed of bridged crystals. High-molecular-weight PAAs (Mw: 90000 and 250000) drastically decreased the grain size as a strong capping agent and promoted the formation of thin films. The array of PAA on the solid surface induced two-dimensional growth of $CaCO_3$ crystals. In this case, the solid surface covered with PAA acted as a template for control of the macroscopic forms. However, low-molecular-weight PAA could not adsorb on a negatively charged glass surface

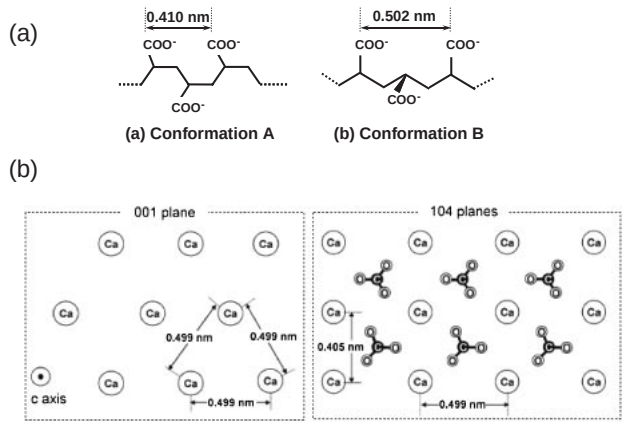

Fig. 12. Schematic illustration of PAA (a) and atomic arrangement of two kinds of calcite planes (b). Reproduced from Ref. 93 with permission of the American Chemical Society.

under neutral and basic conditions, in which $CaCO_3$ crystals are grown. The presence of nonionic hydroxy groups of chitosan and PVA is effective for the adsorption of low-molecular-weight PAA. On the other hand, high-molecular-weight PAA would be anchored to the surface of a glass substrate due to its high adsorbability. The nucleation of $CaCO_3$ was initiated, and then two-dimensional growth of nanograins was guided by the array of low-molecular-weight PAA on chitosan and PVA or high-molecular-weight PAAs on a glass substrate (macroscopic template effect). The difference in the performance of the PAAs was ascribed to the adsorbability and conformation derived from the polymer chain length. In a binary polymer system (PAA2k and PAA250k), lozenge-shaped films consisting of bridged nanoscale grains were fabricated by a moderate capping effect of a mixture of low- and high-molecular-weight PAAs on a macroscopic template of a glass surface covered with the high-molecular-weight PAA. The distinct habits of crystals consisting of nanograins strongly suggested the presence of bridged crystals incorporated with PAA.

5.1.2 Polymorph Control with Anhydrous Chitosan as a Microscopic Template: The crystal structures or polymorphs of $CaCO_3$, such as calcite, aragonite, and vaterite, are influenced by the conditions for precipitation and the coexistence of impurities in an aqueous solution. While calcite is a thermodynamically stable form in the ambient condition, an increase in the degree of supersaturation in an aquatic system promotes the formation of metastable vaterite. The substitution of Ca^{2+} with Mg^{2+} or Co^{2+} in the carbonate structure has been reported to be effective in the preferential formation of aragonite.[94,95] Thus, aragonite films were selectively produced by the addition of Mg^{2+} to the chitosan–PAA system.[8] In recent years, the selective formation of the metastable polymorphs using organic agents has been studied in order to develop artificial biomimetic systems. Although calcite was grown on a porphyrin monolayer in a system containing PAA as a soluble agent,[14] aragonite and vaterite were obtained on a poly(vinyl alcohol) (PVA) substrate with PAA and poly(glutamic acid) (PGlu), respectively.[11] An eggshell membrane, which is a natural template, was also reported to induce the formation of aragonite and vaterite films in the presence of PGlu and poly(aspartic acid) (PAsp), respectively.[96] In these cases, arrays of organic molecules on a substrate influenced the arrangement of the microscopic atomic lattice as a template (microscopic template effect). However, the selectivity of the polymorphism has been insufficient because the crystal structure was reported to be highly sensitive to environmental conditions such as temperature.[97] Nevertheless, the essence of the comprehensive control of the polymorphism of $CaCO_3$ by regulation with organic molecules has not been clarified.

Table 1. Dependence of the Crystal Structures of Calcium Carbonate Films[a] on the Substrate, Molecular Weight of PAA, and Temperature

PAA/substrate	Temperature/°C			
	10	15	25	35
2k/chitosan	C	$V_{(C)}$	$V_{(C)}$	A V
90k/chitosan	V	V	A V	$A_{(V)}$
250k/chitosan	V	V	—	$A_{(V)}$
90k[b]/glass	—	—	C[c]	—

a) A: aragonite, C: calcite, V: vaterite, —: no data, ( ): a minor component. b) $C_{PAA90k} = 7.2 \times 10^{-2}$ wt %. c) The temperature of the solutions was not strictly controlled.

As described above, pure calcite was grown on a glass substrate in the presence of PAA. In contrast, the existence of various organic substrates as a template frequently produced a mixture of calcite, aragonite, and vaterite. Here, we successfully controlled the crystal structure of $CaCO_3$ films grown on 260 °C-baked chitosan using PAA.[98] Selective production of a particular crystal structure was achieved by variation of the molecular weight of PAA and the temperature of the solution, as listed in Table 1. Although calcite films were basically produced on a glass substrate in the presence of high-molecular-weight PAA, the preferential production of metastable phases, such as aragonite and vaterite, was achieved by the arrangement of PAA anchored to the annealed chitosan surface. A long chain of high-molecular-weight PAAs was arranged on the lattice of the chitosan crystal and promoted the nucleation of specific $CaCO_3$ crystals. It was reported that anhydrous chitosan was formed by baking at temperatures above 240 °C.[99] The distinct rectangular lattice of chitosan or anhydrous chitosan would be suitable for the nucleation of orthorhombic aragonite rather than trigonal calcite. The arrangement of high-molecular-weight PAAs on a 260 °C-baked chitosan at a relatively high temperature promoted the nucleation of aragonite with a strict control of the rectangular structure as a microscopic template. The array of low-molecular-weight PAA or high-molecular-weight PAA arranged at a relatively low temperature resulted in the lateral growth of vaterite. Intense X-ray signals of the (110) and (300) planes indicated that the *c* axis of vaterite in the films laid on the surface of chitosan. The rectangular lattice of the *bc* plane of vaterite (b: 8.56 Å) is close to the array of hydroxy groups of anhydrous chitosan (a: 8.50 and b: 8.62 Å). Thus, weak guidance by chitosan initiated the nucleation of vaterite in which the *c* axis was parallel to the surface. The polymorph of the whole bridged crystal is governed by the structure of the initial grain at the nucleation site on the chitosan surface.

5.1.3 Subsequent Overgrowth with Inherited Crystallo-

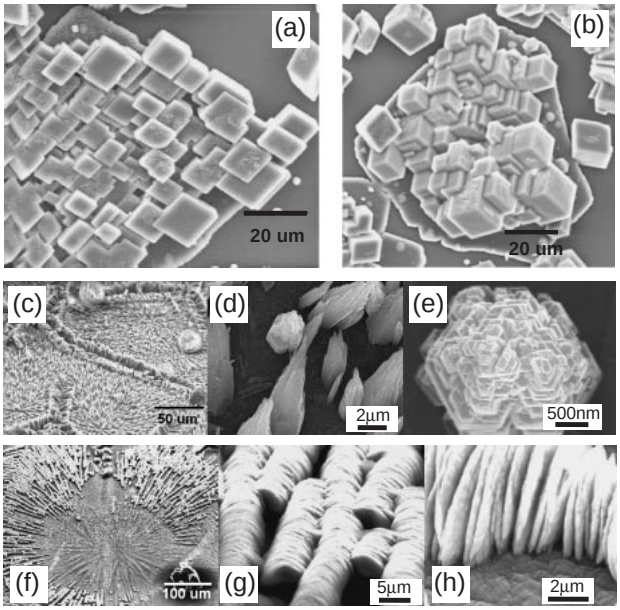

Fig. 13. Subsequent growth of $CaCO_3$ in the absence of PAA. Calcite on the lozenge-shaped films in the absence of any additives.[93,100] Calcite crystals grew either with the {10–14} faces parallel to the film (a) or with the [0001] direction perpendicular to the film (b). Aragonite hexagonal rods on an aragonite film obtained for 1 day with 2.4×10^{-3} wt % of PAA90k (c, d, e) Vaterite high-aspect walls on a vaterite film obtained for 9 h with 2.4×10^{-3} wt % of PAA2k. (f, g, h). Reproduced from Ref. 93 with permission of the American Chemical Society.

graphic Properties: Subsequent growth of PAA-mediated $CaCO_3$ films was performed in a freshly prepared calcium chloride aqueous solution without PAA.[100] The planar morphology of the films evolved into three-dimensional forms by the subsequent growth. The evolution of the morphology was clearly dependent on the polymorphs and crystallographic orientation of the base films as shown in Fig. 13. We observed two types of calcite grains in the directions of ⟨10–14⟩ and [0001] on the surface of the films (Figs. 13a and 13b). The different forms indicate the lozenge-shaped films were grown along the {10–14} or (0001) plane. A forest of hexagonal needles appeared on the aragonite films prepared on an anhydrous chitosan substrate (Figs. 13c–13e). A pseudo-hexagonal morphology was generally observed through the elongation of aragonite along the *c* axis. High-aspect thin walls of ca. 200 nm in thickness and ca. 5 μm in height were aligned along the diameter line of the vaterite films (Figs. 13f–13h). The arrangement of the walls perpendicular to the surface is in agreement with the fact that the *c* axis of the basal vaterite crystals was parallel to the surface. Fundamentally, the crystal structure of the daughter crystals was inherited from the basal films regardless of the condition of the precursor solution.

It is well known that the capping effect of the soluble agents resulted in the formation of films through the suppression of upward crystal growth from the substrate. Here, upward growth was permitted by the subsequent immersion in a supersaturated solution without PAA. The polymorphs and the orientation of the daughter crystals were basically inherited from the base films. The coverage of PAA molecules was unlocked, and the morphology subsequently evolved through epitaxial growth on the surface of the base crystals. Thus, the polymorphs and the orientation are not changed during the subsequent growth process regardless of the presence of PAA. Moreover, the subsequent overgrowth showed that the crystallographic orientation of the nanocrystals composing the macroscopic films was fundamentally the same. These facts indicate that the daughter crystals and nanograins in the basal films were crystallographically bridged like the nanocrystals in biominerals. Since the grain growth freely occurred in the absence of PAA, the habits depending on the polymorphs were clearly exhibited on the daughter crystals.

5.1.4 Development of Nanocrystals into Acute Spines and Hollow Horns: We obtained structural analogues of biominerals, such as calcite spines and cones, composed of small PAA-mediated grains with a preferred crystallographic orientation in a binary system of PAA2k and PAA250k.[101] As mentioned in the previous section, lozenge-shaped calcite films were observed in the binary system with a specific ratio of PAA2k and PAA250k. When the amount of PAA250k was relatively low, calcite mainly formed round rhombohedra on a glass substrate in the initial stage (in a couple of days). Then, spines grew on the previously deposited pedestals in the latter stage (>6 days) (Figs. 14a–14d). The direction of most of the spines was also perpendicular to the face assigned to the {10–14}. According to SEM and TEM observations, the spines were found to consist of small, bridged grains 10–20 nm in diameter. A spot pattern of electron diffraction assignable to {10–14} and (0006) suggested that the small units were arranged with a specific crystallographic orientation (Fig. 14d). Under similar conditions, we found various types of tapering morphologies, such as cones and hollow horns (Figs. 14e–14h). These tapering structures also consisted of small oriented nanocrystals. Although similar morphologies have reportedly been produced by self-assembly of $BaCrO_4$ and $BaSO_4$ nanofibers,[18,20] the formation mechanism is still unclear.

Acute spines and hollow cones consisting of bridged nanocrystals were formed after a long-term reaction. A parabolic shape at the top of the cones was frequently observed in the initial stage. The curvature is ideally produced through crystal growth in a diffusion field. Thus, the formation of the tapering morphology is tentatively ascribed to the presence of a diffusion field. As illustrated in Fig. 15, the consumption of the solutes near the crystal surface with the crystal growth produces a concentration gradient. In the diffusion field, a relatively convex part of the surface can grow faster than the other parts because of the greater concentration gradient at the top of the convex part. Then, tapering morphologies are induced by amplification of fluctuation of the surface. The oriented architecture is achieved by the sequential growth through mineral bridges along specific directions in the diffusion field.

5.2 Growth of Carbonate Crystals in Cooperation with Silicate. 5.2.1 Hierarchical Structures Covered with Silicate: Soluble inorganic anions exhibited capping effects similar to the organic anions in the morphogenesis of carbonate crystals. García-Ruiz et al. published the first reports on the morphological evolution of $CaCO_3$ in the presence of silicate anions.[73a,73b,102,103] We modified their reaction system and

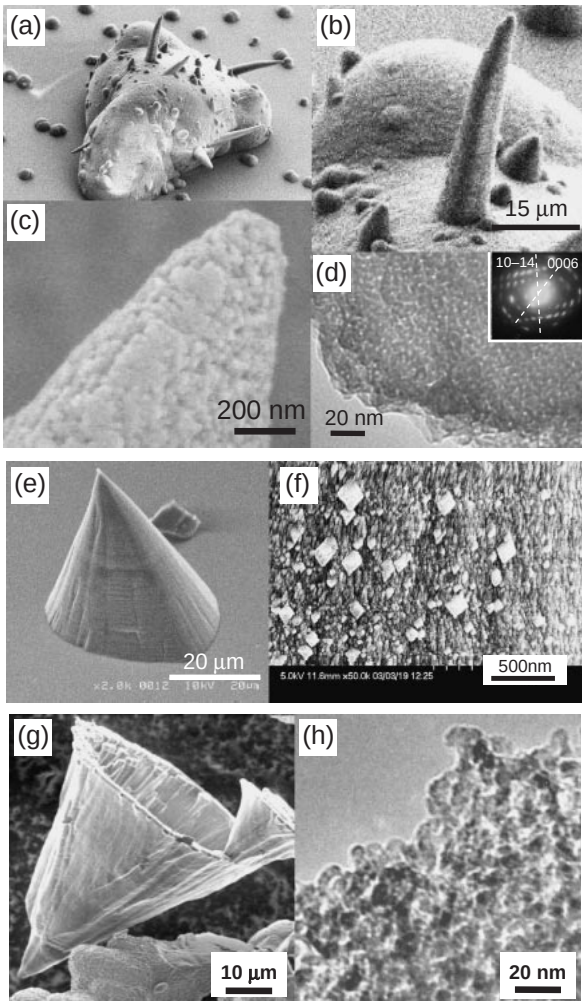

Fig. 14. Development of spines, cones, and hollow horns of $CaCO_3$.[101] SEM images of typical spines grown on round rhombohedral pedestals in the binary system of 2.4×10^{-3}–2.4×10^{-2} wt % (0.33–3.3 mM) PAA2k and 7.2–8.6×10^{-2} wt % (10–12 mM) PAA250k for 8 days (a, b). An enlarged SEM image (c) of the top and a TEM image (d) of the fracture of a spine. SEM images of typical cones obtained in a binary system of 2.4×10^{-3}–2.4×10^{-2} wt % (0.33–3.3 mM) PAA2k and 7.2–8.6×10^{-2} wt % (10–12 mM) PAA250k for 8 days (e, f). A SEM image (g) and a TEM image (h) of a hollow horn of vateraite. Reproduced from Ref. 98 with permission of the American Chemical Society.

found several fascinating morphologies.[104–107] As shown in Figs. 16a and 16b, we obtained many small, three-pointed stars 1 to 5 μm wide attached to the primary star of calcite grown in silica gel at pH 10.5. The secondary star-like units consisted of smaller three-pointed stars 100 to 500 nm wide. The SEM observation indicates that this calcite had a hierarchical structure composed of star-like units arranged with the same crystallographic orientation.

Silicate anions exist in solutions under a highly basic condition. The results of FT-IR suggested that polymerized silicate was adsorbed on the calcite surface. Then bridged, miniaturized three-pointed stars were produced with the polymeric silicate anions. The influence of the silicate anions on the crystal growth might increase because the concentrations of calcium cations and carbonate anions decreased due to the formation of $CaCO_3$. A gradual increase in the influence of silicate anions resulted in the formation of a hierarchical self-similar morphology consisting of three-pointed stars with sizes ranging from 100 nm to $\approx$100 μm. The formation of the small, bridged crystalline units with silicate anions was fundamentally similar to those formed with PAA, although the morphology depended on the specificity of the adsorption of the polymeric anions.

Aragonite occasionally precipitated in silica gel whereas calcite was dominantly produced under this condition. Although hexagonal rods, which are a regular form of aragonite, were obtained in the absence of silicate, coral-like porous morphologies with nanoscale cellular framework (Figs. 16c and 16d) were found in the presence of silicate anions at pH 10.5. Platy units of aragonite in the porous structures were individually covered with silicate envelopes. When aragonite needle crystals were previously added into the silica gel as seeds, we obtained mainly the cellular aragonite. Spherical clusters of the cellular structures were produced around the seed, and then coral-like projections were formed through outgrowth, inheriting the crystallographic properties from the seed. Polymeric silicate was suggested to cover specific surfaces along the *c* axis of aragonite to promote the formation of miniaturized platy units. Sheets and helical forms were produced with aragonite-type $SrCO_3$ and $BaCO_3$ in silica gel under a basic condition (Figs. 16e and 16f). These units were found to be composed of bridged nanocrystals enveloped with silicate (Figs. 16g and 16h). These results suggest that various morphologies were constructed by sequential, bridged growth of carbonate crystals in cooperation with inorganic polymeric anions, as well as organic polymers. The presence of silica gel

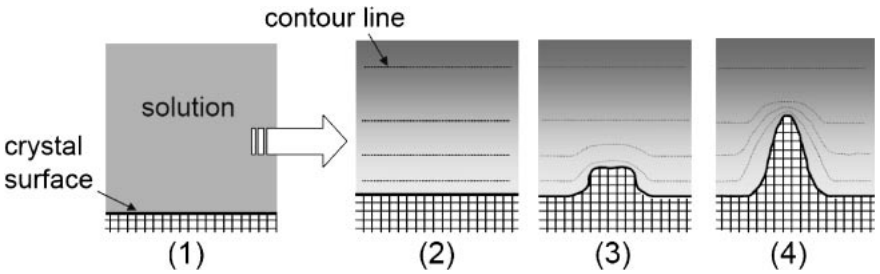

Fig. 15. Schematic illustration of preferential crystal growth under a diffusion-limited condition. The consumption of solutes near the surface with crystal growth produces a concentration gradient in the latter stage (1, 2). Fluctuation of the surface increases with a high concentration gradient at the tip (3, 4). Then, a convex shape is formed on the surface.

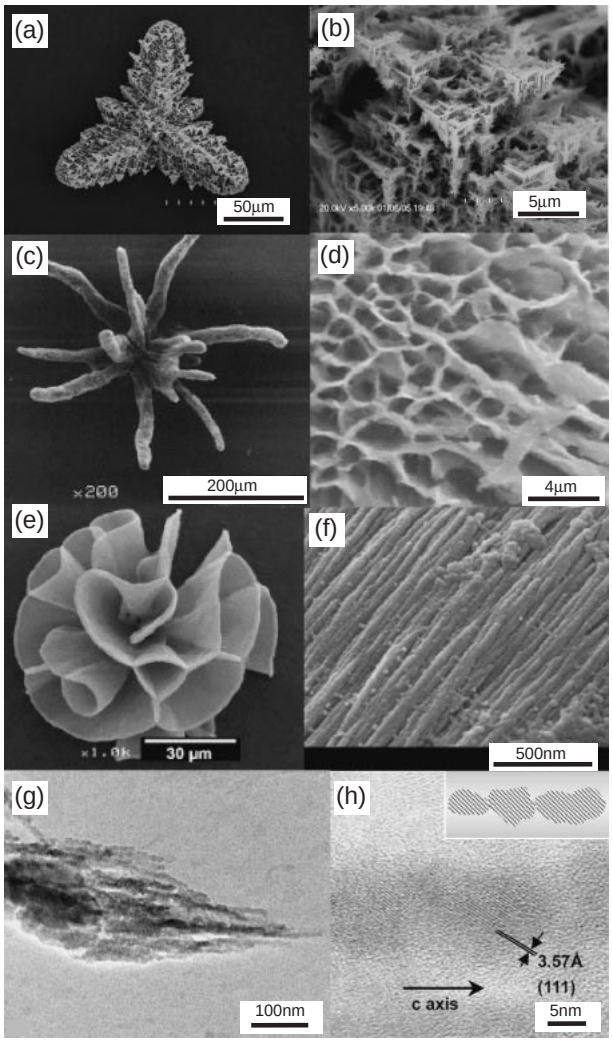

Fig. 16. $CaCO_3$ and $SrCO_3$ crystals grown in the presence of silicate.[105–107] A calcite crystal showing three-fold rotation symmetry (a, b), coral-like morphology of aragonite (c, d) and petal-like $SrCO_3$ (e, f) produced with silica gel at pH 10.5. TEM images of a bundle of fibrous subunits (g) and a fibril (h) in a petal of $SrCO_3$. Reproduced from Refs. 105–107 with permission of the Royal Society of Chemistry and Elsevier.

simultaneously causes a matrix effect for diffusion-controlled mass transport.

5.2.2 Planar Films of Carbonate Crystals with Silicate on Chitosan: We obtained $CaCO_3$ films on a chitosan surface in an aqueous solution system containing silicate anions at pH 10.5.[108] As shown in Figs. 17a and 17b, a planar film was found to be composed of small, bridged units 50–100 nm in diameter. Since silicate was suggested to cover the small crystal grains, the presence of silicate anions in the solution miniaturized the carbonate crystals. The formation of planar films was induced through a 2D arrangement of the small, bridged units on the surface of a chitosan substrate as a macroscopic template. As described in the previous section, subsequent epitaxial growth was achieved on planar films of $CaCO_3$ in a supersaturated solution without any additives. As a concentric array of thin vaterite walls was formed by subsequent growth,

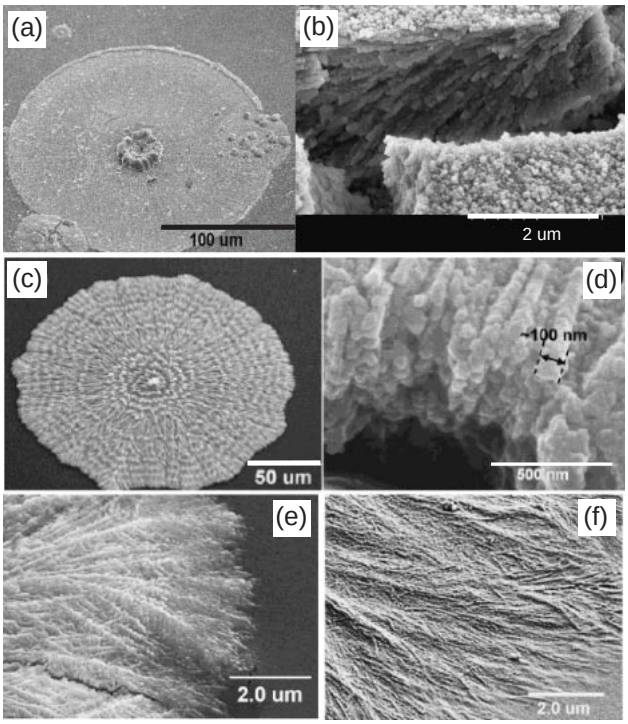

Fig. 17. SEM images of $CaCO_3$ (a, b) and $BaCO_3$ (c–f) planar crystals observed on a chitosan substrate in the presence of silica gel at pH 10.5.[108,109] The edge of barium carbonate planar crystal on a chitosan substrate before (e) and after (f) EDTA treatment. The residue was confirmed to be silica by EDX. Reproduced from Ref. 109 with permission of the American Chemical Society.

the combination of chitosan and silicate anions promoted the nucleation of vaterite in which the *c* axis was parallel to the surface (Fig. 13f).

Aragonite-type carbonates, such as $SrCO_3$ and $BaCO_3$, were also deposited as planar crystals in the presence of silicate anions on a chitosan substrate.[109,110] Planar crystals exhibiting a hexagonal habit were produced through two-dimensional dendritic growth with bridged hexagonal units, in which the *c* axis was arranged perpendicular to the surface (Figs. 17c and 17d). Silicate anions initiated the nucleation of aragonite-type crystals as a template on the insoluble polyalcohol substrate and induced crystal growth of the bridged units as a capping agent. A laminated architecture was constructed through stacking of the platy units with a silica skin, which was confirmed by dissolution of $BaCO_3$ cores with an EDTA solution (Figs. 17e and 17f). These *c*-axis-arranged aragonite layers are similar to nacre in shells, although the thickness of the plates was smaller than that of the bioproducts.

5.3 Overview of the Morphogenesis with Self-Organization with Soluble Polymeric Agents. In the presence of soluble agents, such as PAA and silicate, bridged nanocrystals in cooperation with the cooperative agents were grown. Since the scale of the nanocrystals was not correlated with the size of the components, such as atoms, ions, and molecules, the formation process of the bridged nanocrystals is in the category of self-organization. This fact suggests that the specific adsorption of soluble agents induces the self-organized formation of

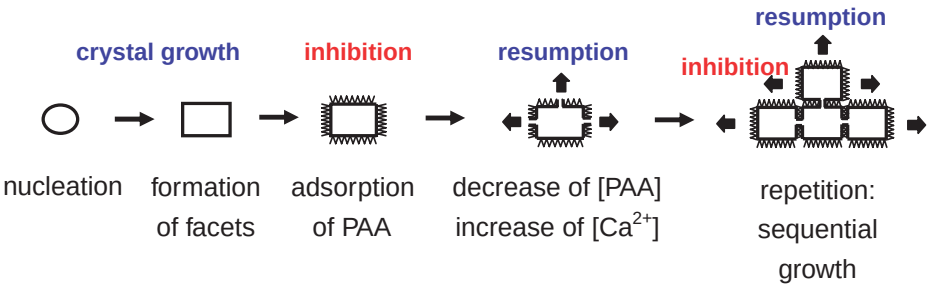

Fig. 18. The sequential growth of bridged units with cooperation of the crystal growth and the inhibition with the adsorption.

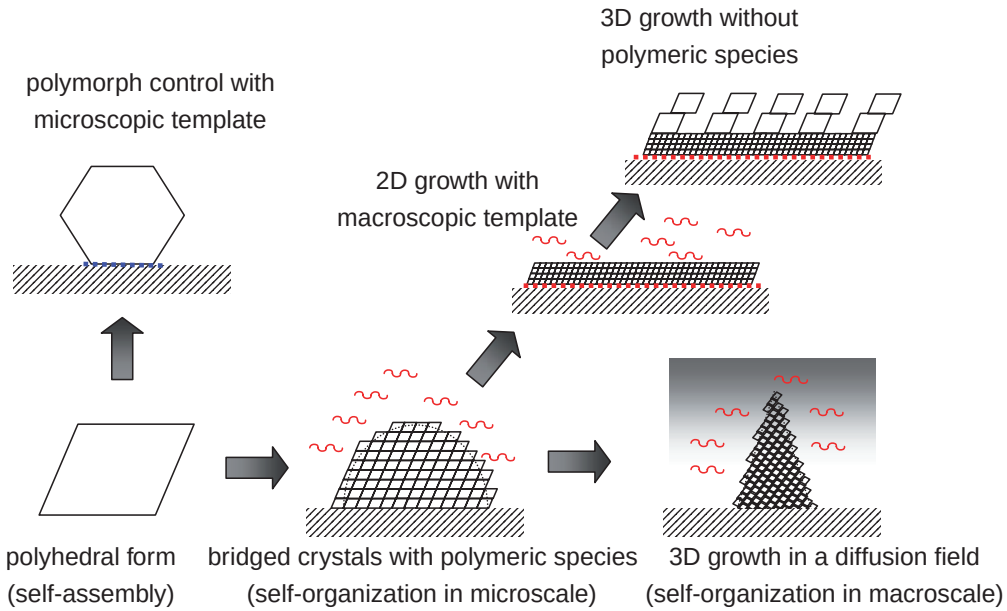

Fig. 19. Overview of morphological evolution with self-assembly and self-organization on crystals growth of calcium carbonate.

hierarchical architectures consisting of small units. Although the specific adsorption of organic molecules having carboxy groups on the surface of $CaCO_3$ crystals has been reported, only crystal habits were changed by monomeric molecules. On the other hand, crystal growth was inhibited by a strong adsorption of polymeric agents, such as PAA and silicate. However, growth resumes when polymeric agents provide a covering because the degree of the supersaturation increases around the surface. The repetition of the inhibition and the resumption of the crystal growth would produce the bridged units. Finally, sequential growth of bridged units is achieved by the cooperation of the crystal growth and the adsorption as shown in Fig. 18. The morphological variation would be easily achieved with a lowering of the surface energy due to adsorption of the cooperative agents. The size of the units were determined by the balance between the crystal growth and the adsorbability. In most biominerals and the mimetic architectures of $CaCO_3$, the size of the units was within 100 nm. Since the specific adsorption occurs on specific faces of the unit crystals, the minimum size of the units may be associated with the formation of the facets exhibiting a habit of the crystal.

Figure 19 illustrates an overview of the morphological evolution of $CaCO_3$ through the self-organization in the presence of polymeric molecules. A rhombohedral form of calcite is the most stable state grown through self-assembly. The crystal structure was varied by the control of the nucleation with a microscopic template effect of the array of PAA or silicate on a substrate (modulation of self-assembly). The coexistence of polymeric anions induced the self-organized formation of small, bridged crystal units with the oriented architecture. The development of the morphology through self-organization was controlled by a macroscopic template effect. Planar structures are produced through two-dimensional growth, guided by a substrate covered with PAA or silicate. Three-dimensional evolution of the bridged crystals is promoted under diffusion-controlled mass transport. The morphological evolution is fundamentally ascribed to the variation of self-assembly into self-organization with capping effects.

Amorphous calcium carbonate (ACC) containing a great amount of organic molecules and inorganic ions has been reported to play an important role in the formation of complex morphologies of crystalline calcium carbonate.[111–115] Actually, the presence of ACC was shown growing at the top of sea urchin spines.[48] The bridged nanocrystals of $CaCO_3$ in biominerals and its mimetic materials may be formed from ACC through the solid–solid transformation. However, the formation of bridged nanocrystals was observed for various crystals other than $CaCO_3$. Consequently, the presence of the amorphous phase is not essential for the nanoscale engineering of the morphogenesis via self-organization on the crystal growth.

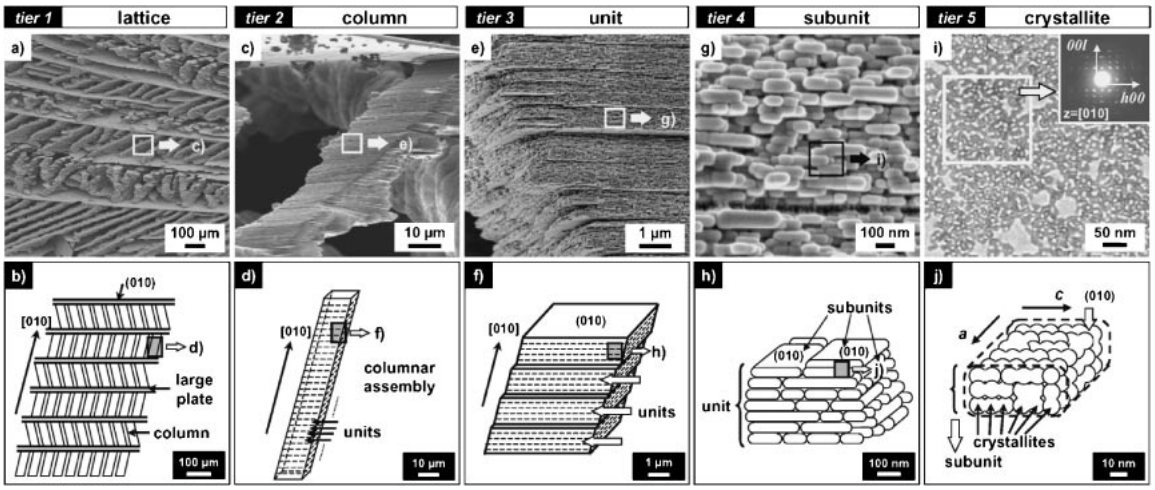

Fig. 20. Hierarchical superstructure consisting of K_2SO_4 and PAA organized on five levels from nanoscopic to macroscopic.[118] Overview of the hierarchical architecture and its schematic illustration in six different scales ($C_{PAA} = 10\,g\,dm^{-3}$). a and b) SEM image and the schematic representation of the macroscopic lattice architecture consisting of large thin plates and columns (tier 1), c and d) columnar assembly between plates (tier 2), e and f) units in the columns (tier 3), g and h) subunits inside of a unit (tier 4), i and j) TEM image and schematic representation of the crystallites with the same orientation in a subunit (inset: corresponding SAED patterns taken along the [010] direction, tier 5). Reproduced from Ref. 118 with permission of Wiley-VCH.

6. Hierarchical Crystal Growth

6.1 Formation of Hierarchical Architectures with a Soluble Polymer. We show a novel type of hierarchically organized superstructures emerging from an exquisite association of inorganic crystals and organic polymers through simple biomimetic crystallization. Potassium sulfate (K_2SO_4) was prepared in an aqueous solution containing PAA with evaporation of water.[116–118] The resultant superstructure consisting of K_2SO_4 and PAA was hierarchically organized on five levels from nanoscopic to macroscopic. Figure 20 shows SEM images and the schematic representation of the macroscopic lattice architecture (tier 1), columns between plates (tier 2), platy units in the columns (tier 3), granular subunits inside of a unit (tier 4), and crystallites (TEM image) with the same orientation in a subunit (inset: corresponding SAED (selected area electron diffraction) patterns taken along the [010] direction, tier 5). A hierarchically organized architecture on multiple scales was also generated from potassium hydrogen phthalate crystals and PAA with an exquisite association of polymers on crystallization.[119] In accordance with these two model cases, the concept for crystal growth can be applied to the generation of a hierarchically organized architecture regardless of whether organic or inorganic materials are used. Our findings shed light on the nature of hierarchical crystal growth in various biominerals, such as bone and mother of pearl. Furthermore, tailoring the combination of crystals and polymers could bring about various hierarchically organized materials with emergent properties that are unattainable with the individual components.

6.2 Formation of Macroscopic Structures. The resulting material was totally mineralized and was integrated on a macroscopic scale (tier 1) regardless of PAA concentration. Thin plates were observed at a relatively low PAA concentration. A habit modification of PAA fundamentally led to the thin plate of K_2SO_4, mainly exhibiting the (010) faces. As the PAA concentration increased, columnar assemblies in tier 2 were produced between the primary plates by sequential growth perpendicular to the (010) faces (Figs. 21a–21c). Consequently, a macroscopic lattice architecture was obtained by alternative growth of the plates and the columns. While the number of thin plates was reduced, the morphological evolution of the columnar growth proceeded with a further increase in the PAA concentration. The columnar growth with the platy units changed to a zigzag architecture via turning and/or branching in a specified direction. Finally, curved, twisted, and helical morphologies emerged under diffusion-controlled mass transport in a similar manner to helical forms in a gel matrix described in the previous section.[116] The modulation of the bridged growth of the platy units in tier 3 made up various morphologies in tier 2.

6.3 Formation of Microscopic Structures. The inside of a platy unit had a two-tiered structure with the same orientation (tiers 4 and 5) (Figs. 21d–21f). A platy unit in tier 3 consisted of the layered subunits (tier 4). Detailed observation using SEM and TEM images indicated that the subunits were also composed of crystallites with a diameter of 10–20 nm (tier 5), regardless of the PAA concentration. Since TEM observations and the subsequent SAED patterns showed a spot pattern, the crystallites were highly aligned in the (010) plane with the same orientation. Therefore, a platy unit in tier 3 was composed of the two-tiered bridged subunits (tier 4) and crystallites (tier 5). The bridged architecture was determined to be due to self-organized formation with the capping effect of PAA.

6.4 The Dual Role (Matrix and Capping Effects) of a Soluble Polymer. We found that PAA molecules were incorporated with K_2SO_4 in two different ways. About 20 wt % of PAA molecules served as the "strongly incorporated PAA," which resulted in habit modification through specific adsorption on the crystal faces. The large thin plate (tier 1) and the platy unit of columnar assembly (tier 3) were eventually formed by habit modification. The excess amount of polymer acted as a growth medium leading to a diffusion-controlled

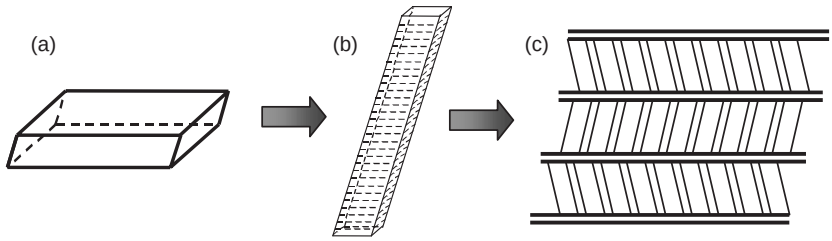

Fig. 21. Schematic illustration of the formation of hierarchical architectures of inorganic–organic composites mimicking biominerals through self-organized crystal growth in several scales.

mass transport and then was simply attached to the K_2SO_4 crystal surface after the evaporation of water ("simply attached PAA," about 80 wt %). As mentioned above, diffusion-controlled growth has a great potential for designing the crystal morphology. An increase in the PAA concentration mainly contributed to an increase in the amount of attached PAA and produced diffusion-controlled conditions leading to helical and twisted morphologies consisting of the bridged units (tier 2).

The incorporated PAA played important roles in the structure of tiers 4 and 5. An increase in the initial concentration of PAA resulted in a slight increase in the incorporated PAA. Since the thickness and the arrangement of subunits were controlled by the PAA concentration, the bridged growth of the subunits (tier 4) and the crystallites (tier 5) was ascribed to self-organization in cooperation with PAA. Viewed from the nanoscopic scale, the selective adsorption leading to habit modification results from the electrostatic interaction between the carboxy groups of PAA and the potassium ions on the (010) face of K_2SO_4. An increase in the incorporated PAA segmentalizes the bridged units on the tier 5 scale. Coupling of strong crystal–polymer interactions and diffusion-controlled conditions that are mediated by the dual roles of PAA is required for construction of the hierarchical architectures.

As mentioned in the previous section, nanostorage for organic molecules is generated by electrostatic interactions between nanocrystal bricks and biopolymer mortars in real biominerals. An anionic dye molecule actually occupied the space in a hierarchically organized composite of K_2SO_4/PAA. Thus, we identified the ability of the hierarchical architecture to host organic molecules. Consequently, a biomimetic architecture in terms of hierarchy, oriented structure, and nanostorage has been generated through self-organized growth of K_2SO_4 and PAA. These results imply that a versatile nanoengineering strategy using bridged bricks and mortars can be adopted for the construction of bioinorganic architectures.

7. Conclusion

Understanding the biomineralization processes as self-organization is important to reproduce the biomimetic architectures. In an artificial system mimicking biomineralization, the morphologenesis of inorganic crystals on several scales is fundamentally achieved by self-assembly at the atomic level and self-organization at the microscopic and macroscopic levels. Figure 22 illustrates that the multi-scale structures would be precisely controlled by the combination of the matrix, capping, and template effects with organic and/or polymeric species. If strong interactions mainly occur in the system, the incorporated polymer induces habit modification for zero- and two-dimensional architectures, such as nanoparticles and nanowires. The absence of strong interaction only results in the diffusion-controlled morphogenesis as shown in Fig. 1. When the versatile effects of the organic and/or polymeric species are coupled during the crystal growth, hierarchically organized architecture is formed. A similar strategy can be employed in bioinorganic superstructures that are directed by controlled crystallization with the assistance of biological molecules and polymers. The emergence of macroscopic and microscopic sequential growth modes with bridged units and guidance for the construction of the units with a template is an essential strategy for the biomimetic approach through self-organization.

In recent years, functional oxides, such as titanium(IV) dioxide, tin oxide, and zinc oxide, were prepared in an aqueous system mimicking biomineralization.[120–122] The general concept of bridged nanocrystals would be applicable as a novel type of inorganic crystals and inorganic–organic nanocomposite materials. Thus, the strategy of the bridged nanocrystals in cooperation with organic agents would be utilized to fabricate a wide variety of functional materials. The formation process through self-organization is a possible new paradigm for advanced material processing.

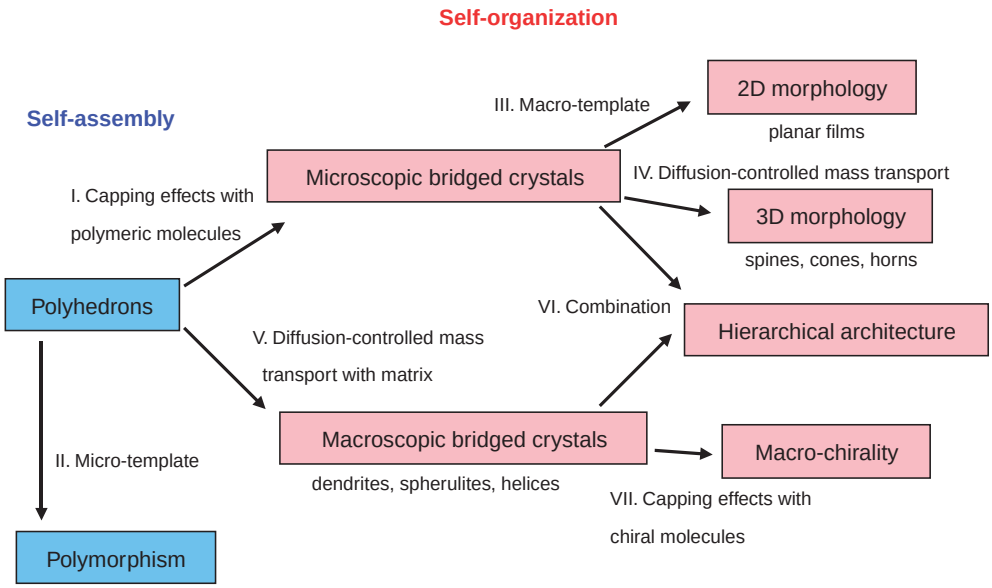

Fig. 22. Schematic illustration of the formation of various architectures of inorganic crystals through self-organization with molecular species. The specific adsorption of soluble agents induces the self-organized formation of hierarchical architectures consisting of small units (I). The control of the nucleation determining the polymorph of the whole crystal is ascribed to a microscopic template effect derived from the lattice matching between an inorganic crystal and organic molecules on the surface of a substrate (II). A flat surface of a substrate promoted the formation of a film through two-dimensional growth of the bridged nanocrystals (III). The oriented architecture would be achieved by the sequential growth through mineral bridges along specific directions in the diffusion field (IV). Convection-free matrices of gel and viscous liquid easily suppress mass transport and promote the self-organized growth with a diffusion-controlled growth mode through the suppression (V). The emergence of macroscopic and microscopic sequential growth modes with bridged units and guidance for the construction of the units with a template is inferred to be the essential strategy for the biomimetic approach through self-organization (VI). The control of the self-organization, such as macroscopic chiral tuning, is achieved by a specific adsorption of a soluble agent on the crystal surface through molecular recognition (VII).

We are grateful to Mrs. T. Terada, T. Miura, and R. Ise for their cooperation. This work was supported by Grant-in-Aid for Scientific Research (No. 15560587) and 21st Century COE program "KEIO Life Conjugated Chemistry" from the Ministry of Education, Culture, Sports, Science and Technology, Japan. One of the authors (Y. O.) is grateful for JSPS research fellowship for young scientists.

References

1 J. Hulliger, *Angew. Chem., Int. Ed. Engl.* **1994**, *33*, 143, and references therein.
2 J. Aizenberg, J. C. Weaver, M. S. Thanawala, V. C. Sundar, D. E. Morse, P. Fratzl, *Science* **2005**, *309*, 275.
3 M. Sumper, E. Brunner, *Adv. Funct. Mater.* **2006**, *16*, 17.
4 Examples of key reviews: a) S. Mann, *Biomineralization*, Oxford University Press, Oxford, **2001**. b) S. Mann, *Angew. Chem., Int. Ed.* **2000**, *39*, 3392. c) S. Weiner, L. Addadi, *J. Mater. Chem.* **1997**, *7*, 689. d) G. A. Ozin, *Acc. Chem. Res.* **1997**, *30*, 17. e) S. Mann, G. A. Ozin, *Nature* **1996**, *382*, 313. f) S. Mann, *Nature* **1993**, *365*, 499. g) L. Addadi, S. Weiner, *Angew. Chem., Int. Ed. Engl.* **1992**, *31*, 153. h) S. Mann, D. D. Archibald, J. M. Didymus, T. Douglas, B. R. Heywood, F. C. Meldrum, N. J. Reeves, *Science* **1993**, *261*, 1286.
5 T. Kato, A. Sugawara, N. Hosoda, *Adv. Mater.* **2002**, *14*, 869.
6 T. Kato, T. Amamiya, *Chem. Lett.* **1999**, 199.
7 T. Kato, T. Suzuki, T. Irie, *Chem. Lett.* **2000**, 186.
8 A. Sugawara, T. Kato, *Chem. Commun.* **2000**, 487.
9 N. Hosoda, T. Kato, *Chem. Mater.* **2001**, *13*, 688.
10 A. Sugawara, T. Ishii, T. Kato, *Angew. Chem., Int. Ed.* **2003**, *42*, 5299.
11 N. Hosoda, A. Sugawara, T. Kato, *Macromolecules* **2003**, *36*, 6449.
12 S. Zhang, K. E. Gonsalves, *Langmuir* **1998**, *14*, 6761.
13 B. R. Heywood, S. Mann, *J. Am. Chem. Soc.* **1992**, *114*, 4681.
14 G. Xu, N. Yao, I. A. Aksay, J. T. Groves, *J. Am. Chem. Soc.* **1998**, *120*, 11977.
15 L. B. Gower, D. J. Odom, *J. Cryst. Growth* **2000**, *210*, 719.
16 Examples of recent key reviews: a) H. Cölfen, *Curr. Opin. Colloid Interface Sci.* **2003**, *8*, 23. b) S. H. Yu, H. Cölfen, *J. Mater. Chem.* **2004**, *14*, 2124. c) H. Cölfen, S. Mann, *Angew. Chem., Int. Ed.* **2003**, *42*, 2350. d) S. Mann, *Chem. Commun.* **2004**, 1.
17 For metal carbonates: a) J. M. Marentette, J. Norwig, E. Stockelmann, W. H. Meyer, G. Wegner, *Adv. Mater.* **1997**, *9*, 647. b) H. Cölfen, L. Qi, *Chem. Eur. J.* **2001**, *7*, 106. c) S. H. Yu, H. Cölfen, J. Hartmann, M. Antonietti, *Adv. Funct. Mater.* **2002**, *12*, 541. d) S. H. Yu, H. Cölfen, A. W. Xu, W. Dong, *Cryst. Growth Des.* **2003**, *4*, 33. e) S. H. Yu, H. Cölfen, M. Antonietti, *J. Phys. Chem. B* **2003**, *107*, 7396. f) M. J. Olszta, S. Gajjerman, M. Kaufman, L. B. Gower, *Chem. Mater.* **2004**, *16*, 2355. g) J. Rudloff, H. Cölfen, *Langmuir* **2004**, *20*, 991. h) J. Yu, J. C. Yu, L. Zhang, X. Wang, L. Wu, *Chem. Commun.* **2004**, 2414. i) N. Nassif, N. Gehrka, N. Pinna, N. Shirshova, K. Tauer, M. Antonietti, H. Cölfen, *Angew. Chem., Int. Ed.* **2005**, *44*, 6004.
18 For barium sulfates: a) L. Qi, H. Cölfen, M. Antonietti, M.

Li, J. D. Hopwood, A. J. Ashley, S. Mann, *Chem. Eur. J.* **2001**, *7*, 3526. b) L. Qi, H. Cölfen, M. Antonietti, *Angew. Chem., Int. Ed.* **2000**, *39*, 604. c) L. Qi, H. Cölfen, M. Antonietti, *Chem. Mater.* **2000**, *12*, 2392. d) H. Cölfen, L. Qi, Y. Mastai, L. Börger, *Cryst. Growth Des.* **2002**, *2*, 191.

19 For calcium phosphate: a) A. Bigi, E. Boanini, D. Walsh, S. Mann, *Angew. Chem., Int. Ed.* **2002**, *41*, 2163. b) M. Antonietti, M. Breulmann, C. G. Göltner, H. Cölfen, K. K. Wong, D. Walsh, S. Mann, *Chem. Eur. J.* **1998**, *4*, 2493.

20 For barium chromates: a) S. H. Yu, H. Cölfen, M. Antonietti, *Chem. Eur. J.* **2002**, *8*, 2937. b) S. H. Yu, M. Antonietti, H. Cölfen, J. Hartmann, *Nano Lett.* **2003**, *3*, 379.

21 For zinc oxide: Z. R. Tian, J. A. Voigt, J. Liu, B. Mckenzie, M. J. Mcdermott, *J. Am. Chem. Soc.* **2002**, *124*, 12954.

22 a) D. K. Kondepudi, I. Prigogine, *Dissipative Structures* in *Modern Thermodynamics: From Heat Engines to Dissipative Structures*, John Wiley & Sons, New York, **1998**, Chap. 19, pp. 427–457. b) I. R. Epstein, J. A. Pojman, *An Introduction to Nonlinear Chemical Dynamics: Oscillations, Waves, Patterns, and Chaos*, Oxford University Press, Oxford, **1998**. c) E. Ben-Jacob, P. Garik, *Nature* **1990**, *343*, 523.

23 Y. Saito, T. Ueta, *Phys. Rev. A* **1989**, *40*, 3408.

24 A key review for mesocrystal: H. Cölfen, M. Antonietti, *Angew. Chem., Int. Ed.* **2005**, *44*, 5576, and references therein.

25 Recent key reports for mesocrystal: a) S. Wohlrab, N. Pinna, M. Antonietti, H. Cölfen, *Chem. Eur. J.* **2005**, *11*, 2903. b) X. T. Wang, H. Cölfen, M. Antonietti, *J. Am. Chem. Soc.* **2005**, *127*, 3246.

26 Recent key reports for oriented attachment: a) R. L. Penn, J. F. Banfield, *Science* **1998**, *281*, 969. b) R. L. Penn, J. F. Banfield, *Geochim. Cosmochim. Acta* **1999**, *63*, 1549. c) J. Polleux, N. Pinna, M. Antonietti, M. Niederberger, *Adv. Mater.* **2004**, *16*, 436. d) C. Pacholski, A. Kornowski, H. Weller, *Angew. Chem., Int. Ed.* **2002**, *41*, 1181. e) B. Liu, S. H. Yu, L. Li, F. Zhang, Q. Zhang, M. Yoshimura, P. Shen, *J. Phys. Chem. B* **2004**, *108*, 2788. f) M. Niederberger, F. Krumeich, K. Hegetschweiler, R. Nesper, *Chem. Mater.* **2002**, *14*, 78.

27 For the nacreous layer: N. Watabe, *J. Ultrastruct. Res.* **1965**, *12*, 351.

28 A. P. Jackson, J. F. V. Vincent, R. M. Turner, *Proc. R. Soc. London, Ser. B* **1988**, *234*, 415.

29 M. Sarikaya, *Microsc. Res. Tech.* **1994**, *27*, 360.

30 P. Calvert, S. Mann, *J. Mater. Res.* **1988**, *23*, 3801.

31 L. Addadi, S. Weiner, *Nature* **1997**, *389*, 912.

32 T. E. Schäffer, C. Ionescu-Zanetti, R. Proksch, M. Fritz, D. A. Walters, N. Almqvist, C. M. Zaremba, A. M. Belcher, B. L. Smith, G. D. Stucky, D. E. Morse, P. K. Hansma, *Chem. Mater.* **1997**, *9*, 1731.

33 E. DaiMasi, M. Sarikaya, *J. Mater. Res.* **2004**, *19*, 1471.

34 B. A. Gotliv, L. Addadi, S. Weiner, *ChemBioChem* **2003**, *4*, 522.

35 Y. L. Kalisman, G. Falini, L. Addadi, S. Weiner, *J. Struct. Biol.* **2001**, *135*, 8.

36 T. Kato, *Adv. Mater.* **2000**, *12*, 1543.

37 Y. Levi, S. Albeck, A. Brack, S. Weiner, L. Addadi, *Chem. Eur. J.* **2006**, *4*, 389.

38 For stereom of sea urchin: K. M. Towe, *Science* **1967**, *157*, 1048.

39 J. D. Currey, D. Nichols, *Nature* **1967**, *214*, 81.

40 G. Donnay, D. L. Pawson, *Science* **1969**, *166*, 1147.

41 H. U. Nissen, *Science* **1969**, *166*, 1150.

42 P. L. O'Neill, *Science* **1981**, *213*, 646.

43 A. Berman, L. Addadi, S. Weiner, *Nature* **1998**, *331*, 546.

44 J. T. Semeon, P. R. Buseck, *Am. Mineral.* **1993**, *78*, 775.

45 X. Su, S. Kamat, A. H. Heuer, *J. Mater. Res.* **2000**, *35*, 5545.

46 A. Berman, J. Hanson, L. Leiserowitz, T. F. Koetzle, S. Weiner, L. Addadi, *Science* **1993**, *259*, 776.

47 J. Aizenberg, J. Hanson, T. F. Koetzle, L. Leiserowitz, S. Weiner, L. Addadi, *Chem. Eur. J.* **1995**, *1*, 414.

48 Y. Politi, T. Arad, K. Eugenia, S. Weiner, L. Addadi, *Science* **2004**, *306*, 1161.

49 J. Aizenberg, J. Hanson, T. F. Koetzle, S. Weiner, L. Addadi, *J. Am. Chem. Soc.* **1997**, *119*, 881.

50 S. Albeck, J. Aizenberg, L. Addadi, S. Weiner, *J. Am. Chem. Soc.* **1993**, *115*, 11691.

51 J. Seto, Y. Zhang, P. Hamilton, F. Wilt, *J. Struct. Biol.* **2004**, *148*, 123.

52 H. Silyin-Roberts, R. M. Sharp, *Proc. R. Soc. London, Ser. B* **1986**, *227*, 303.

53 Q. L. Feng, X. Zhu, H. D. Li, T. N. Kim, *J. Cryst. Growth* **2001**, *233*, 548.

54 J. Gautron, M. T. Hincke, K. Mann, M. Panheleux, M. Bain, M. D. McKee, S. E. Solomon, Y. Nys, *J. Biol. Chem.* **2001**, *276*, 39243.

55 J. P. Cuif, Y. Dauphin, *J. Struct. Biol.* **2005**, *150*, 319.

56 a) X. Li, W. C. Chang, Y. J. Chao, R. Wang, M. Chang, *Nano Lett.* **2004**, *4*, 613. b) K. Takahashi, H. Yamamoto, A. Onoda, M. Doi, T. Inaba, M. Chiba, A. Kobayashi, T. Taguchi, T. Okamura, N. Ueyama, *Chem. Commun.* **2004**, 996.

57 a) I. Sethmann, A. Putnis, O. Gransmann, P. Löbmann, *Am. Mineral.* **2005**, *90*, 1213. b) I. Sethmann, R. Hinrichs, G. Wörheide, A. Putnis, *J. Inorg. Biochem.* **2006**, *100*, 88.

58 J. C. Weaver, L. I. Pietrasanta, N. Hedin, B. F. Chmelka, P. K. Hansma, D. E. Morse, *J. Struct. Biol.* **2003**, *144*, 271.

59 J. Banfield, S. A. Welch, H. Zhang, T. T. Ebert, R. L. Penn, *Science* **2000**, *289*, 751.

60 Y. Oaki, H. Imai, *Angew. Chem., Int. Ed.* **2005**, *44*, 6571.

61 Y. Oaki, H. Imai, *Small* **2006**, *2*, 66.

62 Y. Oaki, S. Hayashi, H. Imai, T. Funatsu, Y. Saikawa, M. Nakata, K. Hashimoto, *Cryst. Growth Des.*, in revision.

63 Y. Oaki, A. Kotachi, T. Miura, H. Imai, *Adv. Funct. Mater.* **2006**, *16*, 1633.

64 H. K. Henisch, *Crystals in Gels and Liesegang Rings*, Cambridge University Press, Cambridge, **1988**.

65 J. Dennis, H. K. Henish, *J. Electrochem. Soc.* **1967**, *114*, 263.

66 M. C. Robert, F. Lefaucheux, *J. Cryst. Growth* **1988**, *90*, 358.

67 A. Cecal, M. Palamaru, A. Juverdeanu, M. Giosan, *J. Cryst. Growth* **1996**, *158*, 181.

68 A. Moreno, G. Juárez-Martínez, T. Hernández-Pérez, N. Batina, M. Mundo, A. McPherson, *J. Cryst. Growth* **1999**, *205*, 375.

69 Y. Oaki, H. Imai, *Cryst. Growth Des.* **2003**, *3*, 711.

70 a) J.-M. Lehn, *Angew. Chem., Int. Ed. Engl.* **1990**, *29*, 1304. b) A. H. Clark, S. B. R. Murphy, *Adv. Polym. Sci.* **1987**, *83*, 57. c) A. E. Rowan, R. J. M. Nolte, *Angew. Chem., Int. Ed.* **1998**, *37*, 63, and references therein.

71 a) W. E. Lindsell, P. N. Preston, J. M. Seddon, G. M. Rosair, A. J. Woodman, *Chem. Mater.* **2000**, *12*, 1572. b) W. Yang, X. Chai, L. Chi, X. Liu, Y. Cao, R. Lu, Y. Jiang, X. Tang, H. Fuchs, T. Li, *Chem. Eur. J.* **1999**, *5*, 1144.

72 a) J. Liu, F. Zhang, T. He, *Macromol. Rapid Commun.*

2001, *22*, 1340. b) Z. Barteczak, A. S. Argon, R. E. Cohen, T. Kowalewski, *Polymer* **1999**, *40*, 2367.

73 For carbonates: a) J. M. García-Ruiz, *J. Cryst. Growth* **1985**, *73*, 251. b) J. M. García-Ruiz, S. T. Hyde, A. M. Carnerup, A. G. Christy, M. J. Van Kranendonk, N. J. Welham, *Science* **2003**, *302*, 1194. c) S. H. Yu, H. Cölfen, K. Tauer, M. Antonietti, *Nat. Mater.* **2005**, *4*, 51.

74 For barium sulfate: a) M. Li, S. Mann, *Langmuir* **2000**, *16*, 7088. b) J. D. Hopwood, S. Mann, *Chem. Mater.* **1997**, *9*, 1819.

75 For potassium dichromate: a) J. Suda, T. Nakayama, A. Nakahara, M. Matsushita, *J. Phys. Soc. Jpn.* **1996**, *65*, 771. b) J. Suda, M. Matsushita, K. Izumi, *J. Phys. Soc. Jpn.* **2000**, *69*, 124. c) J. Suda, M. Matsushita, *J. Phys. Soc. Jpn.* **2004**, *73*, 771.

76 For manganese oxide: O. Giraldo, S. L. Brock, M. Marquez, S. L. Suib, H. Hillhouse, M. Tsapatsis, *Nature* **2000**, *405*, 38.

77 For zinc oxide: a) Z. L. Wang, X. Y. Kong, Y. Ding, P. Gao, W. L. Hughes, R. Yang, Y. Zhang, *Adv. Funct. Mater.* **2004**, *14*, 943. b) X. Y. Kong, Z. L. Wang, *Nano Lett.* **2003**, *3*, 1625.

78 For silica/surfactant composites: a) S. M. Yang, I. Sokolov, N. Coombs, C. T. Kresge, G. A. Ozin, *Adv. Mater.* **1999**, *11*, 1427. b) W. J. Kim, S. M. Yang, *Adv. Mater.* **2001**, *13*, 1191.

79 H. Imai, Y. Oaki, *Angew Chem., Int. Ed.* **2004**, *43*, 1363.

80 R. M. Hazen, D. S. Sholl, *Nat. Mater.* **2003**, *2*, 367.

81 J. Aizenberg, J. Hanson, T. F. Koetzel, S. Weiner, L. Addadi, *J. Am. Chem. Soc.* **1997**, *119*, 881.

82 S. Mann, N. H. C. Sparks, R. P. Blakemore, *Proc. R. Soc. London, Ser. B* **1987**, *231*, 477.

83 C. A. Orme, A. Noy, A. Wiezbicki, M. T. McBride, M. Grantham, H. H. Teng, P. M. Dove, J. J. DeYoreo, *Nature* **2001**, *411*, 775.

84 A. M. Cody, R. D. Cody, *J. Cryst. Growth* **1991**, *113*, 508.

85 Y. Oaki, H. Imai, *J. Am. Chem. Soc.* **2004**, *126*, 9271.

86 R. J. Park, F. C. Meldrum, *Adv. Mater.* **2002**, *14*, 1167.

87 J. Aizenberg, D. A. Muller, J. L. Grazul, D. R. Hamann, *Science* **2003**, *299*, 1205.

88 Y. H. Ha, R. A. Vaia, W. F. Lynn, J. P. Costantino, J. Shin, A. B. Smith, P. T. Matsudaira, E. L. Thomas, *Adv. Mater.* **2004**, *16*, 1091.

89 D. Walsh, S. Mann, *Nature* **1995**, *377*, 320.

90 J. Zhan, H. P. Lin, C. Y. Mou, *Adv. Mater.* **2003**, *15*, 621.

91 T. Kato, T. Suziki, T. Amamiya, T. Irie, M. Komiyama, *Supramol. Sci.* **1998**, *5*, 411.

92 N. Wada, S. Suda, K. Kanamura, T. Umegaki, *J. Colloid Interface Sci.* **2004**, *279*, 167.

93 A. Kotachi, T. Miura, H. Imai, *Chem. Mater.* **2004**, *16*, 3191.

94 Y. Kitano, *Bull. Chem. Soc. Jpn.* **1962**, *35*, 1980.

95 K. Jyonosono, A. Kato, *Inorg. Mater.* **1995**, *259*, 492.

96 P. K. Ajikumar, R. Lakshminarayanan, S. Valiyaveettil, *Cryst. Growth Des.* **2004**, *4*, 331.

97 a) J. Küther, W. Tremel, *Chem. Commun.* **1997**, 2029. b) J. Küther, R. Seshadri, W. Knoll, W. Tremel, *J. Mater. Chem.* **1998**, *8*, 641.

98 A. Kotachi, T. Miura, H. Imai, *Cryst. Growth Des.* **2006**, *6*, 1636.

99 a) K. Okuyama, K. Noguchi, T. Miyazaki, T. Yui, K. Ogawa, *Macromolecules* **1997**, *30*, 5849. b) T. Yui, K. Imada, K. Okuyama, Y. Obata, K. Suzuki, K. Ogawa, *Macromolecules* **1994**, *27*, 7601. c) K. Ogawa, S. Hirano, T. Miyanishi, T. Yui, T. Watanabe, *Macromolecules* **1984**, *17*, 973.

100 A. Kotachi, T. Miura, H. Imai, *Chem. Lett.* **2006**, *35*, 204.

101 T. Miura, A. Kotachi, Y. Oaki, H. Imai, *Cryst. Growth Des.* **2006**, *6*, 612.

102 T. Baird, P. S. Braterman, P. Chen, J. M. García-Ruiz, R. D. Peacock, A. Reid, *Mater. Res. Bull.* **1992**, *27*, 1031.

103 J. M. García-Ruiz, *Geology* **1998**, *26*, 843.

104 H. Imai, S. Yamabi, T. Terada, N. Shikazono, H. Hirashima, *Trans. Mater. Res. Soc. Jpn.* **2000**, *25*, 469.

105 H. Imai, T. Terada, T. Miura, S. Yamabi, *J. Cryst. Growth* **2002**, *244*, 200.

106 H. Imai, T. Terada, S. Yamabi, *Chem. Commun.* **2003**, 484.

107 T. Terada, S. Yamabi, H. Imai, *J. Cryst. Growth* **2003**, *253*, 435.

108 A. Kotachi, T. Miura, H. Imai, *Chem. Lett.* **2003**, *32*, 820.

109 A. Kotachi, H. Imai, *Cryst. Growth Des.* **2004**, *4*, 725.

110 A. Kotachi, T. Miura, H. Imai, *Trans. Mater. Res. Soc. Jpn.* **2004**, *29*, 2257.

111 L. Addadi, S. Raz, S. Weiner, *Adv. Mater.* **2003**, *15*, 959.

112 D. Volkmer, M. Harms, L. Gower, A. Zigler, *Angew. Chem., Int. Ed.* **2005**, *44*, 639.

113 a) E. Loste, F. C. Meldrum, *Chem. Commun.* **2001**, 901. b) E. Loste, R. J. Park, J. Warren, F. C. Meldrum, *Adv. Funct. Mater.* **2004**, *14*, 1211.

114 J. Rieger, J. Thieme, C. Schmidt, *Langmuir* **2000**, *16*, 8300.

115 A. W. Xu, Y. Qiu, W. F. Dong, M. Antonietti, H. Cölfen, *Adv. Mater.* **2005**, *17*, 2217.

116 Y. Oaki, H. Imai, *Langmuir* **2005**, *21*, 863.

117 Y. Oaki, H. Imai, *Trans. Mater. Res. Soc. Jpn.* **2005**, *30*, 353.

118 Y. Oaki, H. Imai, *Adv. Funct. Mater.* **2005**, *15*, 1407.

119 Y. Oaki, H. Imai, *Chem. Commun.* **2005**, 6011.

120 For titanium(IV) dioxides and its related materials: a) K. Shimizu, H. Imai, H. Hirashima, K. Tsukuma, *Thin Solid Films* **1999**, *351*, 220. b) S. Yamabi, H. Imai, *Chem. Mater.* **2002**, *14*, 609. c) H. Uchiyama, H. Imai, *Chem. Commun.* **2005**, 6014. d) Y. Takezawa, H. Imai, *Small* **2006**, *2*, 390.

121 For zinc oxides: a) S. Yamabi, H. Imai, *J. Mater. Chem.* **2002**, *12*, 3773. b) H. Imai, S. Iwai, S. Yamabi, *Chem. Lett.* **2004**, *33*, 768. c) S. Yamabi, J. Yahiro, S. Iwai, H. Imai, *Thin Solid Films* **2005**, *489*, 23. d) T. Kawano, H. Imai, *J. Cryst. Growth* **2005**, *283*, 490.

122 For tin oxides: H. Ohgi, T. Maeda, E. Hosono, S. Fujihara, H. Imai, *Cryst. Growth Des.* **2005**, *5*, 1079.

Hiroaki Imai was born in Tokyo in 1960. He was graduated from Keio University in 1983 with B.S. degree in applied chemistry. He received his Ph.D. degree in applied chemistry from Keio University in 1990. After working at Nippon Sanso Cooperation, he joined the Department of Applied Chemistry, Faculty of Science and Technology, Keio University as a Research Associate in 1993 and was promoted to an Associate Professor in 1999. His research interests are biomimetic processing for hierarchically structured functional materials using self-organization and self-assembly.

Yuya Oaki was born in Yokohama in 1979. He studied chemistry at Keio University and received his Ph.D. degree from the same university in 2006 supervised by Hiroaki Imai. He was a research associate of 21st COE program Keio Life Conjugated Chemistry in 2005. He now carries out his postdoctoral research work as a JSPS research fellow in Keio University. His research interest is focused on biomineralization, crystal design with association of organic molecules, synthesis and analysis of nanostructured functional materials.

Akiko Kotachi received her B.S. degree in applied chemistry from Keio University in 1988. For 10 years, she studied synthesis and evaluation of photoresist materials at Fujitsu Limited, before joining Prof. Dr. H. Imai's group. In 2001, as her doctoral studies, she started to study biomimetic material synthesis and completed her Ph.D. in 2005 under the supervision of Prof. Dr. H. Imai at Keio University. The main research interests are establishment of biomimetic processing of inorganic materials, and their practical use. Her current position is an external researcher of Waseda University.